



## Molecular processes mediating hyperhomocysteinemia-induced metabolic reprogramming, redox regulation and growth inhibition in endothelial cells

Michael Jan<sup>a,b</sup>, Ramon Cueto<sup>a,1</sup>, Xiaohua Jiang<sup>a</sup>, Liu Lu<sup>a</sup>, Jason Sardy<sup>a</sup>, Xinyu Xiong<sup>a</sup>, Justine E. Yu<sup>a</sup>, Hung Pham<sup>a</sup>, Mohsin Khan<sup>a</sup>, Xuebing Qin<sup>c</sup>, Yong Ji<sup>d</sup>, Xiao-Feng Yang<sup>a,e</sup>, Hong Wang<sup>a,e,\*</sup>

<sup>a</sup> Center for Metabolic Disease Research, Temple University School of Medicine, Philadelphia, PA, United States

<sup>b</sup> Otsuka Pharmaceutical Development & Commercialization, Inc., Princeton, NJ, United States

<sup>c</sup> Tulane National Primate Research Center, School of Medicine, Tulane University, Covington, LA, United States

<sup>d</sup> Key Laboratory of Cardiovascular Disease and Molecular Intervention, Nanjing Medical University, Nanjing, China

<sup>e</sup> Department of Microbiology and Immunology, Temple University School of Medicine, Philadelphia, PA, United States

### ARTICLE INFO

#### Keywords:

Homocysteine  
Global mRNA/miRNA expression  
Endothelial injury  
Metabolic reprogramming  
Redox signaling  
Inflammation  
Degradation  
Proliferation

### ABSTRACT

Hyperhomocysteinemia (HHcy) is an established and potent independent risk factor for degenerative diseases, including cardiovascular disease (CVD), Alzheimer disease, type II diabetes mellitus, and chronic kidney disease. HHcy has been shown to inhibit proliferation and promote inflammatory responses in endothelial cells (EC), and impair endothelial function, a hallmark for vascular injury. However, metabolic processes and molecular mechanisms mediating HHcy-induced endothelial injury remains to be elucidated. This study examined the effects of HHcy on the expression of microRNA (miRNA) and mRNA in human aortic EC treated with a pathophysiologically relevant concentration of homocysteine (Hcy 500  $\mu$ M). We performed a set of extensive bioinformatics analyses to identify HHcy-altered metabolic and molecular processes. The global functional implications and molecular network were determined by Gene Set Enrichment Analysis (GSEA) followed by Cytoscape analysis. We identified 244 significantly differentially expressed (SDE) mRNA, their relevant functional pathways, and 45 SDE miRNA. HHcy-altered SDE inversely correlated miRNA-mRNA pairs (45 induced/14 reduced mRNA) were discovered and applied to network construction using an experimentally verified database. We established a hypothetical model to describe the biochemical and molecular network with these specified miRNA/mRNA axes, finding: 1) HHcy causes metabolic reprogramming by increasing glucose uptake and oxidation, by glycogen debranching and NAD<sup>+</sup>/CoA synthesis, and by stimulating mitochondrial reactive oxygen species production via NNT/IDH2 suppression-induced NAD<sup>+</sup>/NADP-NADPH/NADP<sup>+</sup> metabolism disruption; 2) HHcy activates inflammatory responses by activating inflammasome-pyroptosis mainly through  $\downarrow$ miR193b $\rightarrow$  $\uparrow$ CASP-9 signaling and by inducing IL-1 $\beta$  and adhesion molecules through the  $\downarrow$ miR29c $\rightarrow$  $\uparrow$ NEDD9 and the  $\downarrow$ miR1256 $\rightarrow$  $\uparrow$ ICAM-1 axes, as well as GPCR and interferon  $\alpha/\beta$  signaling; 3) HHcy promotes cell degradation by the activation of lysosome autophagy and ubiquitin proteasome systems; 4) HHcy causes cell cycle arrest at G1/S and S/G2 transitions, suppresses spindle checkpoint complex and cytokinetic abscission, and suppresses proliferation through  $\downarrow$ miRNA335/ $\uparrow$ VASH1 and other axes. These findings are in accordance with our previous studies and add a wealth of heretofore-unexplored molecular and metabolic mechanisms underlying HHcy-induced endothelial injury. This is the first study to consider the effects of HHcy on both global mRNA and miRNA expression changes for mechanism identification. Molecular axes and biochemical processes identified in this study are useful not only for the understanding of mechanisms underlying HHcy-induced endothelial injury, but also for discovering therapeutic targets for CVD in general.

\* Corresponding author. Center for Metabolic Disease Research, Temple University School of Medicine, 3500 North Broad Street, Philadelphia, PA, 19140, United States.

E-mail address: [hongw@temple.edu](mailto:hongw@temple.edu) (H. Wang).

<sup>1</sup> Co-first author.

<https://doi.org/10.1016/j.redox.2021.102018>

Received 7 April 2021; Received in revised form 13 May 2021; Accepted 19 May 2021

Available online 24 May 2021

2213-2317/© 2021 The Authors.

Published by Elsevier B.V. This is an open access article under the CC BY-NC-ND license

(<http://creativecommons.org/licenses/by-nc-nd/4.0/>).

## 1. Introduction

Epidemiological and experimental studies have confirmed that hyperhomocysteinemia (HHcy), a term for elevated levels of plasma homocysteine (Hcy) ( $\geq 15 \mu\text{M}$ ), is an independent risk for cardiovascular disease (CVD), stroke and other degenerative diseases, such as Alzheimer disease, type II diabetes mellitus and chronic kidney disease [1–7]. Endothelial cells (EC) are the inner layer of blood vessels. Endothelial dysfunction is a hallmark for atherosclerosis and CVD and is the earliest event during atherogenesis [8]. We were the first to establish that HHcy selectively suppresses proliferation and arrests the cell cycle at the G1/S transition in EC [9] by cyclin A transcription suppression via DNA hypomethylation at the cell-cycle dependent element (CDE) suppressor binding site [10]. HHcy also suppresses bone marrow (BM)-derived endothelial progenitor cell mobilization and post-injury endothelial repair leading to enhanced atherosclerosis [11]. Other studies showed that HHcy inhibits growth and promotes EC death through fibroblast growth factor 2 (FGF2) transcription repression [12] and inhibits endothelial progenitor cell proliferation through down-regulation of cyclin A and DNA methyltransferase 1 (DNMT1) expression [13].

We previously characterized endothelial dysfunction in large and small arteries from HHcy mice with cystathionine beta synthase (CBS) gene deficiency and mice fed with a high methionine diet [5,14]. HHcy-related endothelial dysfunction was confirmed and associated with enhanced susceptibility to carotid artery thrombosis in HHcy mice [15].

Endothelial activation is characterized by the induction of adhesion molecules such as intercellular adhesion molecule-1 (ICAM-1), vascular cell adhesion molecule-1 (VCAM-1) and E-selectin, which allow immune cells to adhere and cause tissue inflammation [16]. Hcy ( $100 \mu\text{M}$ ) induced the expression of VCAM-1 in human aortic endothelial cells (HAEC) and enhanced monocyte adhesion to HAEC [17]. The accumulation of S-adenosylhomocysteine (SAH), a Hcy metabolite, induced by dialdehyde, an adenosine analog and a potent SAH hydrolase inhibitor, promoted EC activation via induction of ICAM-1, VCAM-1 and E-selectin in human coronary artery endothelial cells [18].

The concept of HHcy-induced endothelial inflammation is supported by our finding that Hcy, at pathophysiological concentrations ( $500 \mu\text{M}$ ), activated inflammatory pyroptosis and non-inflammatory apoptosis in human umbilical vein endothelial cells (HUVEC) by caspase-1 activation/mitochondrial dysfunction/caspase-9/3 activation signaling [19]. It was reported that L-Hcy, at super-physiological levels (2 mM), induced expression and secretion of inflammatory cytokines IL6, IL8 and TNF $\alpha$  by a cathepsin V activation related mechanism in HUVEC [20].

In terms of metabolic regulation, EC are glycolysis dependent for energy production. In EC, 75–85% of ATP is produced from glycolysis and 15–30% of ATP is produced from oxidation of glucose, fatty acids (FA), and glutamine through oxidative phosphorylation (OXPHOS) [21, 22]. The glycolytic features of EC may be attributed to their access to high oxygen levels in the blood, making EC vulnerable to oxidative stress. ECs rely on glycolysis for energy production instead of OXPHOS because the OXPHOS process would produce high levels of reactive oxygen species (ROS) and potentially disrupt redox homeostasis [23].

In response to insults, cells undergo metabolic reprogramming and redox homeostasis, impairment of which contributes to cell and tissue damage through increased cytotoxicity, autoimmunity, and inflammation [24,25]. We found that HHcy-induced EC-dependent vascular relaxation and apoptosis/pyroptosis in EC are associated with elevated intracellular ROS levels and reversed by antioxidants superoxide dismutase (SOD)/catalase (CAT) [19,26]. In HHcy mice, downregulation of antioxidant pathways mediated by endoplasmic reticulum (ER) glutathione peroxidase 7 (GPx 7) was associated with ER redox imbalance and vasculopathy [27].

We recently proposed a new concept that the Hcy-methionine (HM) metabolic cycle is a key metabolic sensor system that responds to

various risk factors. HM cycle abnormalities lead to the pathological accumulation of HM cycle metabolites, mostly Hcy and SAH, which modulate S-adenosylmethionine (SAM)/SAH-dependent methylation and pathological responses in disease conditions [28]. In addition, we found that Hcy potentially disrupts tissue mitochondrial electron transport chain complex I, leading to the impairment of the electron transfer cascade, and increased the production of mitochondrial ROS (mtROS) [29]. However, molecular processes mediating HHcy-induced metabolic reprogramming and redox regulation have not been systematically investigated.

In this study, we examine global cellular molecular signaling in Hcy treated HAEC to characterize the metabolic and molecular network potentially mediating HHcy-induced EC injury. To this end, messenger RNA (mRNA) and microRNA (miRNA) microarray analyses were performed using comprehensive bioinformatics tools. This study led us to discover systemic and novel molecular signaling by which HHcy contributes to EC injury in CVD and other degenerative diseases.

## 2. Materials and methods

### 2.1. Cell treatment

HAEC (Lonza, Walkersville, MD) were cultured as previously described [9]. Briefly, HAEC were grown in M199 medium (Thermo Scientific, Waltham, MA) containing 20% fetal calf serum (Thermo Scientific),  $50 \mu\text{g/mL}$  endothelial cell growth supplement (BD Biosciences, San Jose, CA), and  $50 \mu\text{g/mL}$  heparin. Cells from passage 6 were used for experiments. Cells were cultured to 80% confluence and then treated for 48 h with  $500 \mu\text{M}$  L-Hcy to mimic severe HHcy seen in homocystinuria patients with CBS deficiency [30] or with control medium. Chemicals, if not otherwise specified, were purchased from Sigma-Aldrich (St. Louis, MO).

### 2.2. Microarray expression profiling in HHcy-treated HAEC

RNA was extracted from three biological replicates for each treatment group using the miRNeasy Mini Kit (Qiagen, Valencia, CA). RNA quality was assessed using the Nanodrop 2000 Spectrophotometer (Thermo Scientific). mRNA microarrays were performed using Affymetrix GeneChip® Human Gene 1.0 ST Arrays and miRNA microarrays were performed using Affymetrix GeneChip® miRNA 1.0 Arrays (Affymetrix, Santa Clara, CA). Pre-processing of microarray data was performed with Partek® Genomics Suite v6.5 (Partek Inc., St. Louis, MO) using a robust multi-array average (RMA) algorithm to interpret the raw signal.

### 2.3. Principal component analysis

Principal component analysis (PCA) was performed to examine the variance of mRNA/miRNA microarrays. PCA revealed a minimal dissimilarity between one particular day of sample collection as compared to the other two days in two microarrays. However, the variation was minimal, and all samples were used for further analysis. Despite Benjamini-Hochberg correction [31], the false discovery rate (FDR) alone could not be used adequately as a cut-off and instead the p-value ( $P$ ) was utilized.

### 2.4. Identification of HHcy-altered significantly differentially expressed (SDE) mRNA/miRNA

Pre-processing of microarray data was performed with Partek® Genomics Suite v6.5 using an RMA algorithm. A Benjamini-Hochberg correction was applied for multiple testing to adjust FDR. All  $P$  were two-sided and  $P < 0.05$  were considered significant. All statistical analyses after pre-processing with Partek® Genomics Suite v6.5 were performed using R v3.0.2. Significantly differentially expressed (SDE)

mRNA/miRNA after treatment with 500  $\mu$ M L-Hcy were defined as those with  $P < 0.05$  and absolute fold change (FC)  $\geq 1.5$ , which were then considered for further analysis. Heatmaps and volcano plots for all SDE mRNA and miRNA were generated using R Studio software v1.1.456 [32] to illustrate expression across biological replicates.

## 2.5. Identification of inversely correlated HHcy-altered miRNA-mRNA pairs

miRtarBase v7.0 [33], an experimentally verified miRNA-mRNA interaction database was utilized to identify SDE miRNA-mRNA matches, which were applied to the microarray dataset to identify

HHcy SDE miRNA and mRNA direction. The increased SDE miRNAs were correlated with the decreased target SDE mRNA and vice versa. Inversely correlated SDE miRNA-mRNA pairs were identified and considered for further analysis.

Identification of HHcy-altered pathway and network (GSEA & Cytoscape analysis).

Gene Set Enrichment Analysis (GSEA) [34] was applied to the entire mRNA microarray dataset to select statistically significant gene sets (pathways). Top pathways were identified based on  $FDR < 0.05$  of the enriched pathways. Core genes in these top pathways were used to screen the mRNA microarray dataset. HHcy-changed mRNA ( $P < 0.05$ ) in these top pathways were used to construct the molecular network

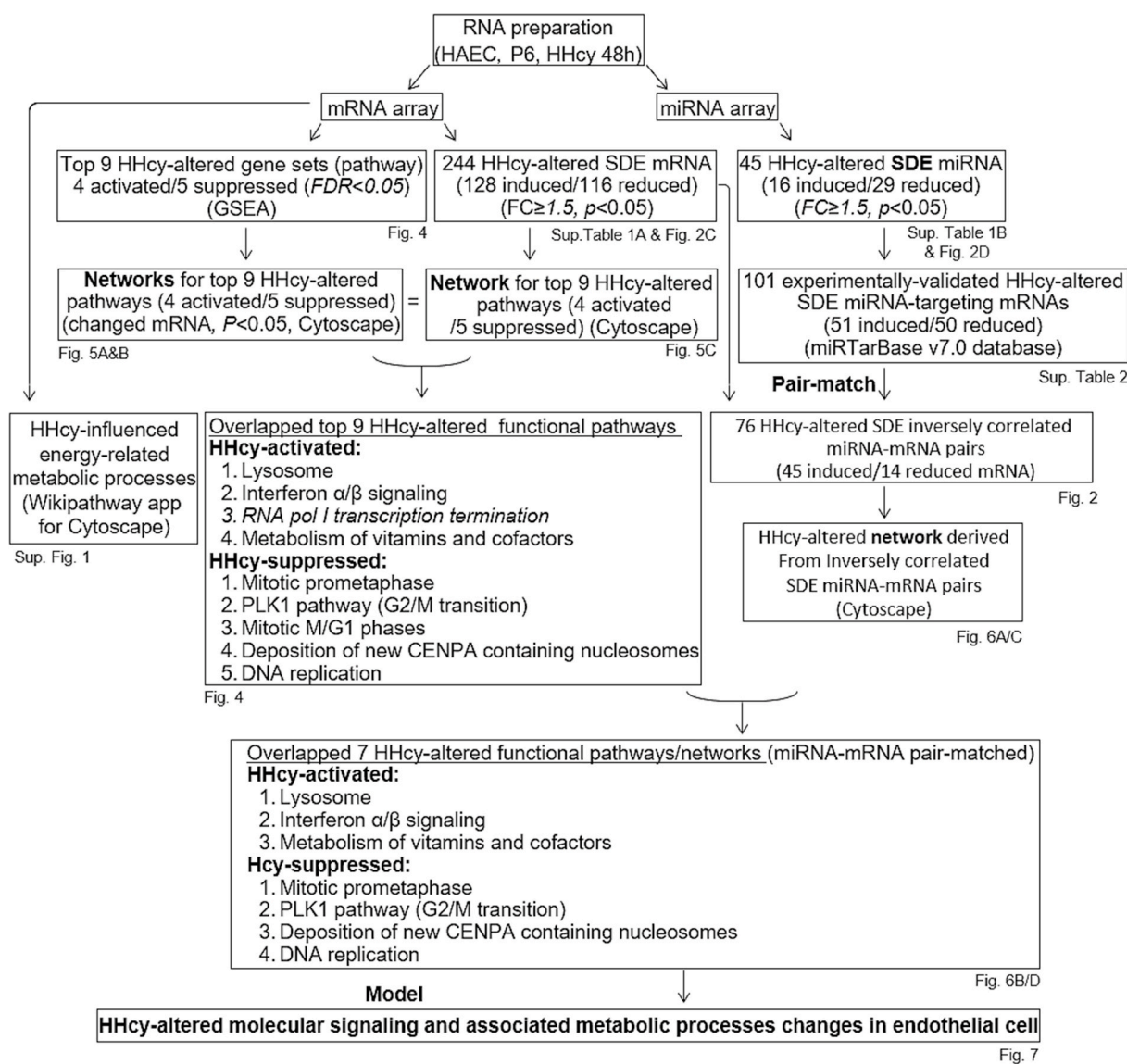


**Fig. 1. Overall strategies to identify HHcy-regulated genes, pathways and molecular processes in endothelial cells.** HAEC (passage 6) grown to 80% confluency were treated with L-Hcy 500  $\mu$ M for 48 h with triplicate samples in each group. mRNA and miRNA were extracted. Affymetrix GeneChip® microarrays were performed. mRNA dataset was analyzed by using Gene Set Enrichment Analysis (GSEA) software to select statistically significant gene sets (pathways) considering  $FDR < 0.05$ . Top 9 HHcy-altered pathways were identified. HHcy-changed mRNAs ( $P < 0.05$ ) from core enrichment genes (Supplementary Table 3) were selected to establish the networks by using ClueGo v2.5.4 and CluePedia v1.5.4 applications in Cytoscape v3.7.1 software. Two hundred forty-four HHcy-altered SDE mRNA ( $FC \geq 1.5, P < 0.05$ ) were identified and used to develop HHcy-altered networks in which the top 9 were overlapped with GSEA pathways. Forty-five HHcy-altered SDE miRNA ( $FC \geq 1.5, P < 0.05$ ) were recognized and used to identify 101 experimentally-validated HHcy-altered miRNA-mRNAs pairs through miRtarBase v7.0 database. Fifty-nine HHcy-altered SDE inversely correlated miRNA-mRNA pairs were identified and used to develop the HHcy-altered networks, in which 7 pathways were recognized in the network identified using mRNA dataset only. HHcy-influenced energy-related metabolic processes were described by incorporating gene expression information in the mRNA dataset using Wikipathway app for Cytoscape v3.7.1 software. Finally, a working model was established to describe molecular pathways and metabolic processes underlying HHcy-induced endothelial injury. Abbreviations: HAEC, human aortic endothelial cells; Hcy, homocysteine; HHcy, hyperhomocysteinemia; miRNA, microRNA; mRNA, messenger RNA; SDE, significantly differentially expressed. FDR, false discovery rate; FC, fold change.

using ClueGo v2.5.4 and CluePedia v1.5.4 from Cytoscape v3.7.1 analyses [35–37].

Cytoscape analysis was also applied to the identified HHcy-altered SDE mRNA and HHcy-altered SDE miRNA inversely matched pairs to construct the molecular networks to add statistical power to the GSEA pathway findings.

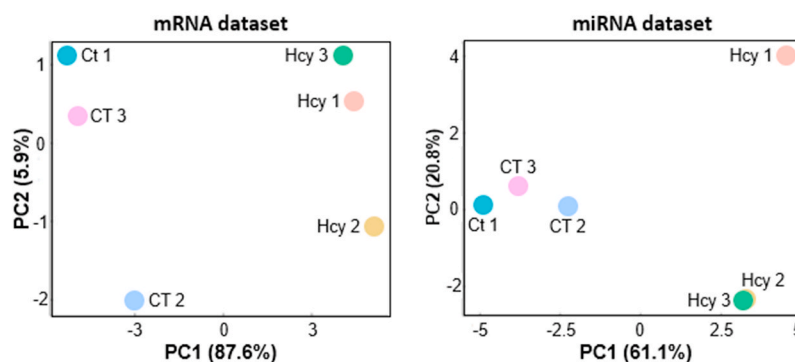
Identification of HHcy-altered metabolic processes (Cytoscape analysis/Wikipathway app).

Five energy-related metabolic processes, including glycolysis, long-chain fatty acid (FA)  $\beta$ -oxidation, glutamate metabolism, tricarboxylic acid (TCA) cycle, and oxidative phosphorylation, were selected to screen the mRNA microarray dataset. HHcy-altered mRNAs were denoted with

### A. Dataset general information

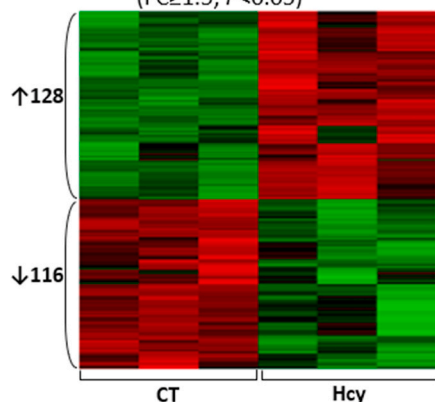
HAEC		
L-Hcy ( $\mu$ M)	0	500
Passage	6	6
Sample #	3	3
Microarray screenings		
Findings	mRNA	miRNA
Denoted	26890	1801
HHcy-SDE	244	45
HHcy-induced	128	16
HHcy-reduced	116	29

### B. Variance analysis (PCA plot)



### C. HHcy-altered SDE mRNA

(FC $\geq$ 1.5;  $P < 0.05$ )



### D. HHcy-altered SDE miRNA

(FC $\geq$ 1.5;  $P < 0.05$ )

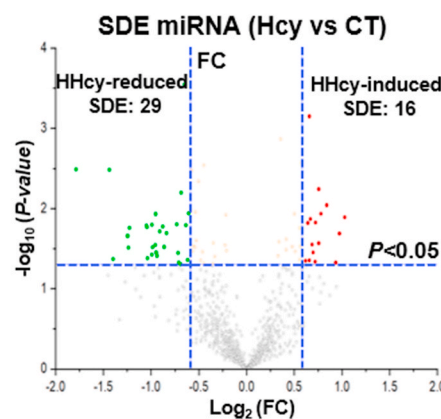
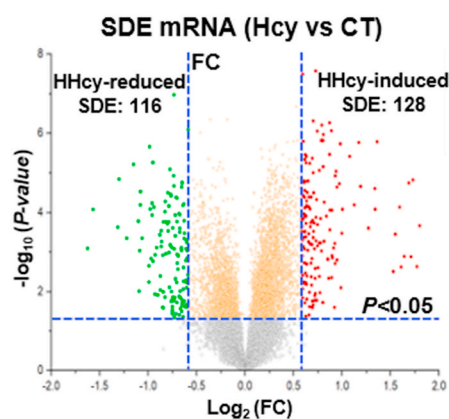
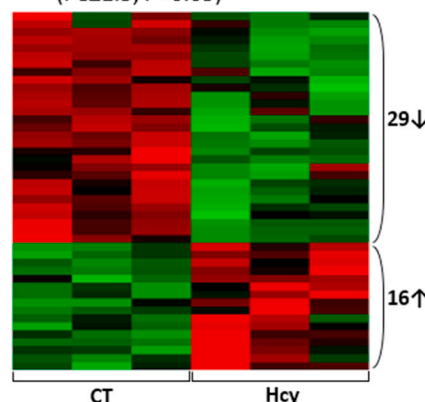


**Fig. 2. Microarray analysis and SDE identification from HHcy-treated HAEC.** A. Dataset general information. HAEC (p6) grown to 80% confluency were treated with 500  $\mu$ M L-Hcy, a concentration representing severe HHcy in humans, for 48 h. mRNA and miRNA were extracted from three biological replicates. Affymetrix GeneChip<sup>®</sup> microarrays were performed. 244 SDE mRNA and 45 SDE miRNA were identified. B. PCA plot. PCA analysis was performed to test data variance integrating top 50 HHcy-altered mRNA/miRNA SDE using RStudio. mRNA PC1 and PC2 are represented by 87.6% and 5.9% variance, respectively. miRNA PC1 and PC2 are represented by 61.1% and 20.8% respectively. C/D. HHcy-altered SDE mRNA/miRNA identification. Heatmap and volcano plot illustrations of HHcy-altered SDE mRNA and miRNA show the expression fold change plotted against the P-Value. Blue dashed lines represent the cut-off of absolute FC  $\geq$  1.50 ( $\text{Log}_2(\text{FC}) \geq 0.58$ ) and  $P < 0.05$ . Filled dots represent SDE mRNA/miRNA. The red filled dots represent HHcy-induced SDE. The green dots represent HHcy-reduced SDE. Abbreviations: FC, fold change; HAEC, human aortic endothelial cells; HHcy, hyperhomocysteinemia; miRNA, microRNA; mRNA, messenger RNA; PCA, principal component analysis; SDE, significantly differentially expressed. (For interpretation of the references to color in this figure legend, the reader is referred to the Web version of this article.)

heatmap color code in the canonical metabolic pathways from the Wikipathway app within Cytoscape v3.7.1 [38].

## 2.6. Model development for HHcy-altered molecular signaling and biochemical processes in EC

The details of the molecular and biochemical connections of HHcy-altered molecular signaling and energy-related metabolic processes were established based on the identified inversely matched HHcy-altered miRNA-mRNA pairs, non-matched SDE mRNAs, changed mRNA and some non-significantly change mRNA to show the trend. The functional implications of HHcy-altered processes are defined based on the current understanding of related gene functions in the literature. A conclusive model for all HHcy molecular and metabolic responses in EC was developed.

## 3. Results

### 3.1. Identification of HHcy-altered SDE mRNA and miRNA

The Affymetrix Gene Chip screening provided denotation for 26,890 mRNA and 1801 miRNA. PCA revealed that PC1 and PC2 accounted for 87.6% and 5.9% of the overall variation in the mRNA microarray dataset, respectively. On the other hand, PCA revealed that PC1 and PC2 accounted for 61.1% and 20.8% of the overall variation in the miRNA microarray dataset, respectively (Fig. 2B).

We identified 244 SDE mRNA and 45 SDE miRNA in 500  $\mu$ M L-Hcy-treated HAEC using the criteria of  $P < 0.05$ , and  $FC \geq 1.5$  (Fig. 1 & 2C/D) and termed these as HHcy-altered SDE mRNA or miRNA, respectively. A complete list with gene names and statistical details for all HHcy-altered SDE mRNA/miRNA is presented in Supplementary Table 1.

Among the 244 HHcy-altered SDE mRNA, there were 128 HHcy-induced and 116 HHcy-reduced SDE mRNA. Among the 45 HHcy-altered SDE miRNA, there were 16 HHcy-induced and 29 HHcy-reduced SDE miRNA. Heatmaps and volcano plots for all HHcy-altered SDE mRNA and miRNA were generated to illustrate expression across biological replicates (Fig. 2C/D).

### 3.2. Identification of 76 inversely matched HHcy-altered miRNA-mRNA pairs

We identified 101 experimentally validated HHcy-altered SDE miRNA-SDE mRNA pairs, including 51 HHcy-induced and 50 HHcy-reduced SDE mRNA, using the miRTarBase v7.0 database. A detailed list for these 101 experimentally validated HHcy-altered SDE miRNA-mRNA pairs are presented in Supplementary Table 2.

Since miRNA functions as a post-transcriptional inhibitor of mRNA expression [39], we only recognized the increased SDE miRNAs that were matched with the decreased target SDE mRNA and vice versa. We identified 76 inversely correlated HHcy-altered miRNA-mRNA pairs as candidates of HHcy-induced miRNA dependent molecular signaling. Among the 76 HHcy-altered SDE miRNA-mRNA inversely matched pairs, 8 HHcy-induced SDE miRNA targeted 14 HHcy-reduced SDE mRNA (19 pairs), and 15 HHcy-reduced SDE miRNA targeted 45 HHcy-induced SDE mRNA (57 pairs) (Fig. 3A/B). The inversely correlated miRNA-mRNA pairs highlighted in quadrants I and III in Fig. 3C were considered for further analysis.

Identification of top 9 HHcy-altered functional pathways (GSEA).

Through GSEA analysis, using the statistical criteria of  $FDR < 0.05$ , we identified 4 severe HHcy-activated functional pathways in the mRNA dataset. These included lysosome, interferon-alpha/beta signaling, RNA polymerase I transcription termination, and metabolism of vitamins/cofactors (Fig. 4A). We also identified 38 severe HHcy-suppressed functional pathways. Interestingly, 35 of 38 (92%) are related to cell cycle regulation. Because of this similarity, we listed the representative top 20 HHcy-suppressed functional pathways in Fig. 4C. We highlighted

the top 5 cell cycle-related HHcy-suppressed functional pathways (mitotic prometaphase, PLK1 pathway, mitotic M/G1 phases, deposition of new CENPA containing nucleosomes and DNA replication), and 2 other pathways (amyloidosis and systemic lupus erythematosus). The enrichment plot in Fig. 4 B/D provides a graphical view of the enrichment score for the top 9 HHcy-altered functional pathways.

HHcy-altered network derived from all HHcy-changed or SDE mRNA (Cytoscape).

Cytoscape analysis provided additional information regarding gene connection and interactions between functional pathways and increased the statistical significance of the GSEA findings. For example, using the HHcy-changed mRNA ( $P < 0.05$ ) extracted from core genes provided by GSEA, we developed the networks for the top 4 HHcy-activated and top 5 HHcy-suppressed functional pathways (Fig. 5A/B).

In HHcy-activated networks, we discovered that HHcy-induced lysosome activation leads to glycosaminoglycan and sphingolipid degradation and that folate biosynthesis, pantothenate, and CoA metabolism are the major metabolic changes. In addition, we identified molecular connections between inflammation and lysosome activation (Fig. 5A). In the HHcy-suppressed network, we identified extensive connections between the top 5 HHcy-suppressed networks and overlapping functions of pathway genes as represented by multicolor pie spheres (Fig. 5B).

We developed an overall network using all 244 HHcy-altered SDE mRNA listed in Supplementary Table 1 and Fig. 5C. We observed that HHcy predominantly (mostly one-color spheres) activated inflammation clusters and metabolic functional groups, and suppressed cell cycle and DNA repair clusters. Interestingly, HHcy uniformly (only one-color spheres) activated lysosome functional groups, also connected with the inflammation cluster, and protein localization to cell surface functional groups. In addition, HHcy also has a uniformly suppressive impact on protein O-glycosylation and peroxisomal membrane functional groups. Most importantly, we were able to find a complete overlap between these three networks and GSEA findings.

HHcy-altered network derived from the inversely correlated SDE miRNA-mRNA pairs (Cytoscape).

We developed two networks, the HHcy-activated network and the HHcy-suppressed network, specifically for the 59 HHcy-altered SDE mRNA that have inversely correlated SDE miRNA (Fig. 3A/B). These networks allowed dissecting the HHcy-altered miRNA-related functional groups.

We observed that the HHcy-activated network integrates broader functional groups compared with the HHcy-suppressed network. In the HHcy-activated network (Fig. 6A), we identified 5 relevant interactive signal pathways, depicted by color, including immune response-inhibiting cell surface receptor pathways, adenylate cyclase-modulating G-protein coupled receptor (GPCR) pathways, chemokine pathways, RANKL/RANK (Receptor activator of NFKB) pathways, and MAP kinase inhibition pathways. On the other hand, the HHcy-suppressed network contained only one functional group, organelle, shown as all green spheres, that describes mostly cell cycle-related daughter functional groups (Fig. 6C), such as cell cycle/cellular process, mitotic phase/cytokinesis, cell division, multicellular organismal process, and intracellular organelle lumen.

Consistently, we identified 3 HHcy-activated functional pathways (Fig. 6B) that were recognized in the top 4 HHcy-activated pathways from GSEA studies (Figs. 1 and 4A/B), including lysosome, interferon  $\alpha/\beta$  signaling, and vitamin metabolism. In addition, we found 4 HHcy-suppressed functional pathways (Fig. 6D) that were previously identified from GSEA, including mitotic prometaphase, PLK1 pathway, deposition of new CENPA containing nucleosomes, and DNA replication (Figs. 1 and 4C/D).

HHcy activated energy metabolism in EC (Cytoscape analysis/Wikipathway app).

We explored HHcy-altered gene expression in 5 energy metabolic processes of interest using Wikipathway app for Cytoscape

**A. 8 HHcy-induced SDE miRNA matched with 14 HHcy-reduced SDE mRNA (19 pairs)**

miRNA	P-value	FC	mRNA Target	P-value	FC
hsa-miR-122-5p	0.0129	2.04	PRR11	0.0058	-1.51
hsa-miR-122-5p	0.0129	2.04	BRCA2	0.0227	-1.57
hsa-miR-122-5p	0.0129	2.04	ENTPD1	0.0001	-1.97
hsa-miR-122-5p	0.0129	2.04	ABCA6	0.0023	-1.99
hsa-miR-122-5p	0.0129	2.04	POGLUT3	0.0002	-2.14
hsa-miR-122-5p	0.0129	2.04	EGFR	0.0001	-1.65
hsa-miR-605-5p	0.0207	1.96	CEP55	0.0316	-1.57
hsa-miR-605-5p	0.0207	1.96	CENPH	0.0008	-1.66
hsa-miR-605-5p	0.0207	1.96	PTGIS	0.0007	-1.71
hsa-miR-325	0.0271	1.69	MMP16	0.0398	-1.60
hsa-miR-497-5p	0.0149	1.65	CEP55	0.0316	-1.57
hsa-miR-497-5p	0.0149	1.65	ENTPD1	0.0001	-1.97
hsa-miR-497-5p	0.0149	1.65	TLL1	0.0028	-1.61
hsa-miR-497-5p	0.0149	1.65	ANLN	0.0176	-1.55
hsa-miR-199b-5p	0.0463	1.65	ZNF117	0.0459	-1.66
hsa-miR-491-5p	0.0281	1.61	HMG2A	0.0014	-1.51
hsa-miR-491-5p	0.0281	1.61	EGFR	0.0001	-1.65
hsa-miR-944	0.0135	1.59	ZNF117	0.0459	-1.66
hsa-miR-514a-3p	0.0007	1.58	CEP55	0.0316	-1.57

**B. 15 HHcy-reduced SDE miRNA matched with 45 HHcy-induced SDE mRNA (57 pairs) (continued)**

miRNA	P-value	FC	mRNA Target	P-value	FC
hsa-miR-335-5p	0.0287	-1.94	CASB	0.0006	1.59
hsa-miR-335-5p	0.0287	-1.94	ABCB9	3.1E-05	1.56
hsa-miR-335-5p	0.0287	-1.94	RNF144A	8.6E-06	1.70
hsa-miR-335-5p	0.0287	-1.94	ASAH1	0.0019	1.60
hsa-miR-335-5p	0.0287	-1.94	SOX17	1.6E-05	1.52
hsa-miR-335-5p	0.0287	-1.94	AKAP12	0.0005	1.66
hsa-miR-335-5p	0.0287	-1.94	CXCR4	2.2E-05	2.28
hsa-miR-411-3p	0.0117	-1.93	IGFBP5	0.0015	1.81
hsa-miR-411-3p	0.0117	-1.93	ADM	3.3E-08	1.51
hsa-miR-519c-3p	0.0303	-1.82	CLEC12B	0.0015	1.81
hsa-miR-29c-3p	0.0203	-1.79	LAMC2	0.0007	1.52
hsa-miR-29c-3p	0.0203	-1.79	NEDD9	0.0006	1.61
hsa-miR-132-3p	0.0158	-1.66	SPRY1	4.3E-06	1.62
hsa-miR-132-3p	0.0158	-1.66	SLC2A1	3.4E-06	1.83
hsa-miR-137	0.0476	-1.63	TRIM13	0.0066	1.55
hsa-miR-137	0.0476	-1.63	TLR3	0.0059	1.54
hsa-miR-181a-5p	0.0064	-1.61	ATP8A1	0.0046	1.65
hsa-miR-181a-5p	0.0064	-1.61	AKAP12	0.0005	1.66
hsa-miR-181a-5p	0.0064	-1.61	PHLDA1	2.8E-05	1.53
hsa-miR-181a-5p	0.0064	-1.61	IL1A	0.0031	2.89
hsa-miR-181a-5p	0.0064	-1.61	CCDC88C	0.0020	1.56
hsa-miR-625-5p	0.0003	-1.57	LYN	0.0008	1.64
hsa-miR-625-5p	0.0003	-1.57	LPCAT3	2.7E-08	1.66
hsa-miR-574-5p	0.0439	-1.53	CCDC88C	0.0020	1.56
hsa-miR-574-5p	0.0439	-1.53	TRIM13	0.0066	1.55
hsa-miR-574-5p	0.0439	-1.53	TRAF5	0.0042	1.70

**B. 15 HHcy-reduced SDE miRNA matched with 45 HHcy-induced SDE mRNA (57 pairs)**

miRNA	P-value	FC	mRNA Target	P-value	FC
hsa-miR-148b-3p	0.0033	-2.70	LAMC2	0.0007	1.52
hsa-miR-148b-3p	0.0033	-2.70	NME5	0.0069	1.61
hsa-miR-148b-3p	0.0033	-2.70	IGFBP5	0.0015	1.81
hsa-miR-148b-3p	0.0033	-2.70	SLC2A1	3.4E-06	1.83
hsa-miR-543	0.0430	-2.63	SIPA1L2	0.0002	1.68
hsa-miR-543	0.0430	-2.63	SHC4	0.0019	1.53
hsa-miR-300	0.0163	-2.07	SIPA1L2	0.0002	1.68
hsa-miR-125a-5p	0.0377	-1.98	PEG10	0.0001	1.53
hsa-miR-125a-5p	0.0377	-1.98	PRDM1	0.0001	2.01
hsa-miR-505-3p	0.0160	-1.98	FAM89A	2.3E-05	1.93
hsa-miR-192-5p	0.0304	-1.98	DUSP16	1.5E-05	1.50
hsa-miR-192-5p	0.0304	-1.98	AGL	0.0175	1.62
hsa-miR-192-5p	0.0304	-1.98	AFAP1L1	0.0001	1.51
hsa-miR-335-5p	0.0287	-1.94	ALDOC	0.0001	1.72
hsa-miR-335-5p	0.0287	-1.94	SORBS2	0.0003	1.58
hsa-miR-335-5p	0.0287	-1.94	DUSP16	1.5E-05	1.50
hsa-miR-335-5p	0.0287	-1.94	IL1A	0.0031	2.89
hsa-miR-335-5p	0.0287	-1.94	SPATA20	1.1E-06	1.75
hsa-miR-335-5p	0.0287	-1.94	CCDC88C	0.0020	1.56
hsa-miR-335-5p	0.0287	-1.94	SHC4	0.0019	1.53
hsa-miR-335-5p	0.0287	-1.94	FAM124B	4.7E-05	1.67
hsa-miR-335-5p	0.0287	-1.94	VASH1	5.7E-06	1.59
hsa-miR-335-5p	0.0287	-1.94	LMCD1	0.0001	1.51
hsa-miR-335-5p	0.0287	-1.94	TRIM16	1.7E-06	2.57
hsa-miR-335-5p	0.0287	-1.94	TSPAN15	6.2E-07	1.73
hsa-miR-335-5p	0.0287	-1.94	SMPDL3A	0.0034	1.54
hsa-miR-335-5p	0.0287	-1.94	TMEM140	1.9E-05	1.96
hsa-miR-335-5p	0.0287	-1.94	VLDLR	0.0002	1.60
hsa-miR-335-5p	0.0287	-1.94	GNA14	0.0003	1.50
hsa-miR-335-5p	0.0287	-1.94	ATP8A1	0.0046	1.65
hsa-miR-335-5p	0.0287	-1.94	DEPP1	0.0001	1.56

**C. HHcy-altered SDE miRNA-mRNA inversely matched pair plot (76 pairs)**

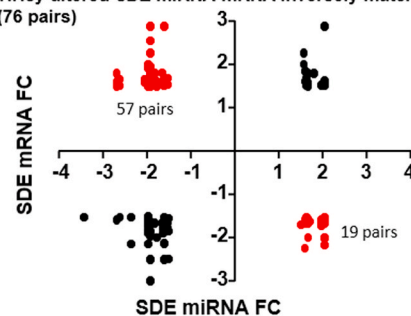
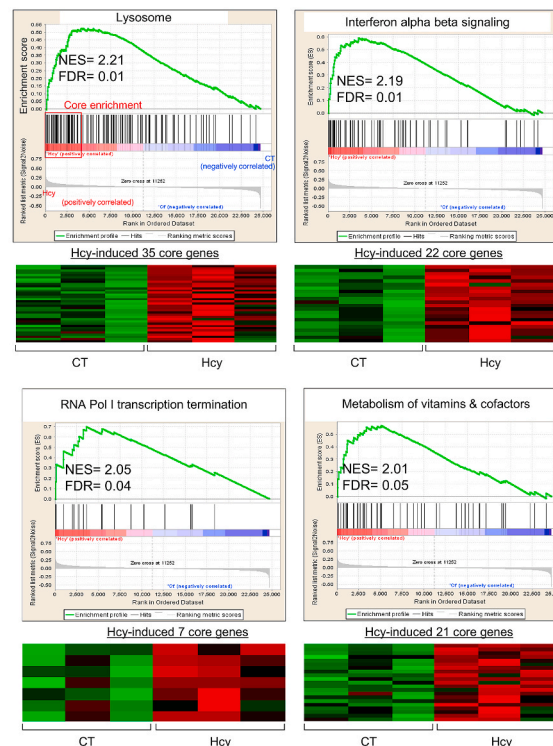


**Fig. 3. Identification of 76 HHcy-altered SDE miRNA-mRNA inversely correlated pairs (45 induced/14 reduced mRNA).** SDE mRNA and miRNA were identified using a cut-off of  $P < 0.05$  and absolute  $FC \geq 1.50$ . Database of experimentally-verified miRNA-mRNA interactions (miRTarBase v7.0) was used. A. 8 HHcy-induced SDE miRNA matched with 14 HHcy-reduced SDE mRNA (19 pairs). B. 15 HHcy-reduced SDE miRNA matched with 45 HHcy-induced SDE mRNA (57 pairs). C. HHcy-altered SDE miRNA-mRNA inversely correlated pair plot (76 pairs). The black dots in the plot represent mRNA-miRNA pairs that share the same direction and the red dots represent inversely correlated pairs. The upper left red dots represent HHcy-induced SDE miRNA targeting HHcy-reduced SDE mRNA, whereas the lower right red dots represent HHcy-reduced SDE miRNA targeting HHcy-induced SDE mRNA. Abbreviations: FC, fold change; HHcy, hyperhomocysteinemia; miRNA, microRNA; mRNA, messenger RNA; SDE, significantly differentially expressed. See full names for gene symbols in [Supplementary Table 1](#). (For interpretation of the references to color in this figure legend, the reader is referred to the Web version of this article.)

**A. Top 20 HHcy-activated pathways from HHcy-induced mRNA (GSEA)**

#	Pathway name - library	NES	NOM p-val	FDR q-val	FWER P-val
1	Lysosome - KEGG	2.21	0.0000	0.0096	0.0080
2	Interferon alpha beta signaling - REACTOME	2.19	0.0000	0.0066	0.0110
3	RNA pol I transcription termination - REACTOME	2.05	0.0000	0.0413	0.1020
4	Metabolism of vitamins and cofactors - REACTOME	2.01	0.0000	0.0478	0.1520
5	Steroid biosynthesis - KEGG	1.93	0.0000	0.1102	0.3710
6	RNA pol I transcription initiation - REACTOME	1.92	0.0000	0.0989	0.3920
7	CD40 pathway - BIOCARTA	1.88	0.0000	0.1259	0.5230
8	RIG I MDA5 mediated induction of IFN $\alpha/\beta$ - REACTOME	1.84	0.0000	0.1666	0.6850
9	MMP cytokine connection - SA	1.83	0.0061	0.1712	0.7360
10	Graft versus host disease - KEGG	1.81	0.0042	0.1918	0.8070
11	IL8 CXCR2 pathway - PID	1.78	0.0039	0.2410	0.9000
12	mRNA capping - REACTOME	1.76	0.0041	0.2619	0.9340
13	Granule cell survival - ST	1.75	0.0039	0.2522	0.9370
14	B cell antigen receptor - ST	1.75	0.0060	0.2493	0.9500
15	IL8 CXCR1 pathway - PID	1.74	0.0117	0.2582	0.9610
16	RNA pol II transcription pre-initiation/promoter opening - REACTOME	1.72	0.0022	0.2666	0.9710
17	Prion diseases - KEGG	1.70	0.0000	0.2938	0.9840
18	Porphyrin and chlorophyll metabolism - KEGG	1.70	0.0104	0.2806	0.9840
19	TRAF6 mediated NF $\kappa$ B activation - REACTOME	1.70	0.0162	0.2666	0.9840
20	Signaling by NOTCH1 - REACTOME	1.69	0.0020	0.2740	0.9880

**B. Gene enrichment plot and heatmap for top 4 HHcy-activated pathways (FDR<0.05)**



**C. Top 20 HHcy-suppressed pathways from HHcy-reduced mRNA (GSEA)**

#	Pathway name/library name	NES	NOM p-val	FDR q-val	FWER P-val
1	Mitotic prometaphase/REACTOME	-2.81	0.0000	0.0000	0.0000
2	Polo-like Kinase 1 (PLK1) - PID	-2.68	0.0000	0.0000	0.0000
3	Mitotic M/G1 phases - REACTOME	-2.61	0.0000	0.0000	0.0000
4	Deposition of new CENPA containing nucleosomes - REACTOME	-2.61	0.0000	0.0000	0.0000
5	DNA replication - REACTOME	-2.54	0.0000	0.0000	0.0000
6	AURORA B- PID	-2.53	0.0000	0.0000	0.0000
7	Cell cycle mitotic - REACTOME	-2.52	0.0000	0.0000	0.0000
8	Cell cycle - REACTOME	-2.51	0.0000	0.0000	0.0000
9	Meiotic recombination - REACTOME	-2.42	0.0000	0.0000	0.0000
10	RNA pol I promoter opening - REACTOME	-2.41	0.0000	0.0000	0.0000
11	Amyloids - REACTOME	-2.35	0.0000	0.0000	0.0000
12	Chromosome maintenance - REACTOME	-2.33	0.0000	0.0000	0.0000
13	Meiosis - REACTOME	-2.25	0.0000	0.0000	0.0000
14	Kinesins - REACTOME	-2.25	0.0000	0.0001	0.0010
15	Packaging of telomere ends - REACTOME	-2.20	0.0000	0.0001	0.0010
16	Forkhead box M1 (FOXM1) - PID	-2.18	0.0000	0.0001	0.0010
17	Systemic lupus erythematosus - KEGG	-2.17	0.0000	0.0001	0.0010
18	Cell cycle - KEGG	-2.16	0.0000	0.0001	0.0030
19	Telomere maintenance - REACTOME	-2.12	0.0000	0.0004	0.0100
20	Meiotic synapsis - REACTOME	-2.11	0.0000	0.0004	0.0100

**D. Gene enrichment plot and heatmap for top 5 HHcy-suppressed pathways (top Cell cycle-related)**

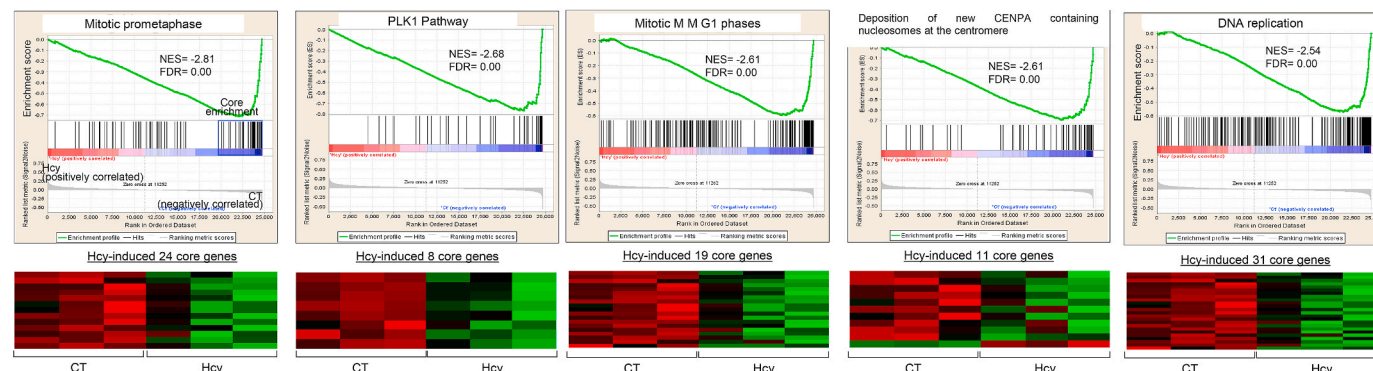
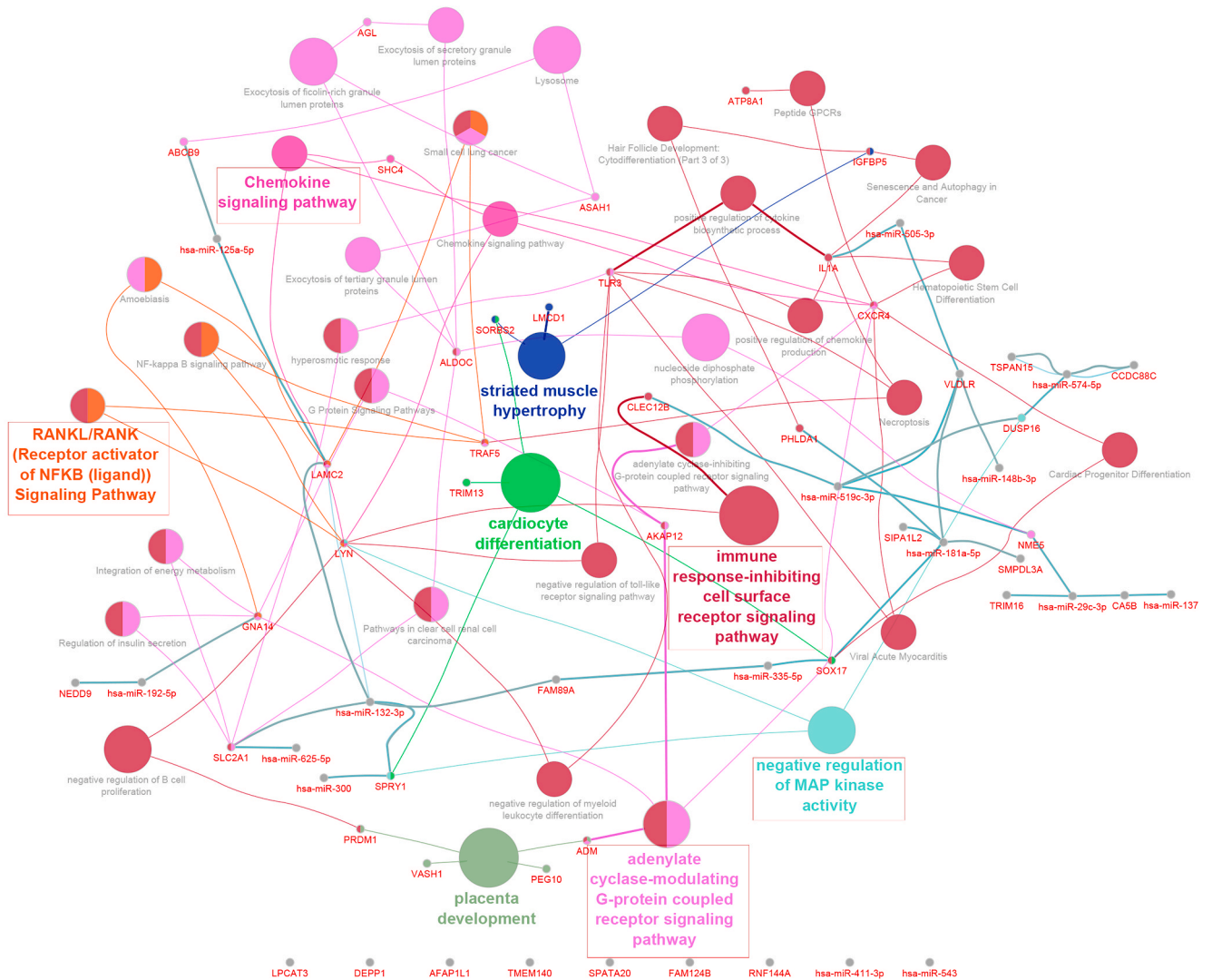


**Fig. 4.** HHcy-altered top pathways, enrichment plot and heatmap (GSEA). mRNA array was analyzed utilizing Gene Set Enrichment Analysis (GSEA). Top pathways were selected based on FDR<0.05. A. Top 20 HHcy-activated pathways from HHcy-induced genes. B. Gene enrichment plot and heatmap for top 4 HHcy-activated pathways (FDR<0.05). C. Top 20 HHcy-suppressed pathways from HHcy-reduced genes. D. Gene enrichment plot and heatmap for top 5 HHcy-suppressed pathways (top list of C. cycle-related and 2 others). Abbreviations: CENPA: centromere protein A; GSEA, gene set enrichment analysis; HHcy, hyperhomocysteinemia; NES, normalized enrichment score; NOM P-val, normalized P-value; FDR, false discovery rate; FWER, familywise-error rate.



**A. Network of HHcy-activated pathways (from HHcy-altered SDE inversely correlated miRNA-mRNA pairs)**

**B. Network of top 3 HHcy-activated pathways (from HHcy-altered SDE inversely correlated miRNA-mRNA pairs)**

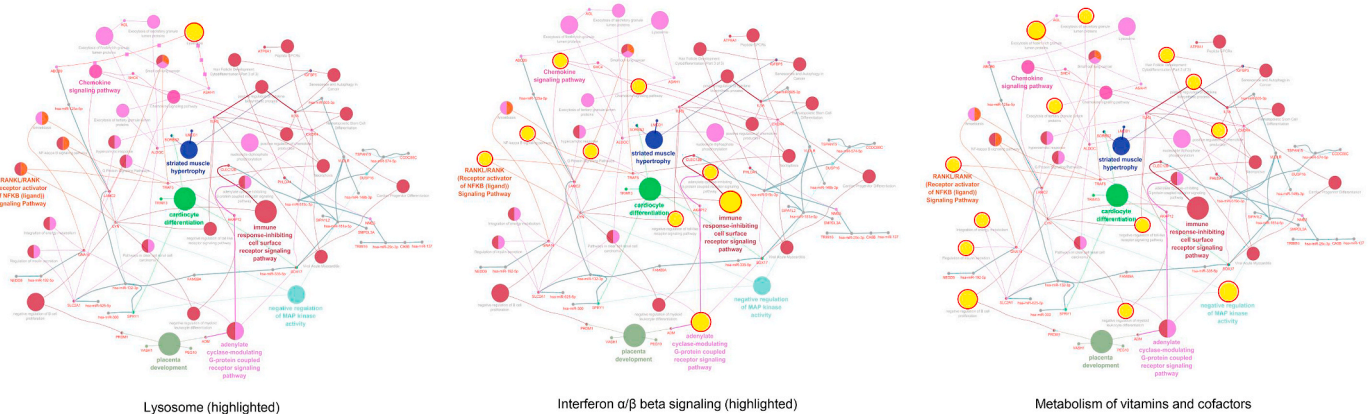
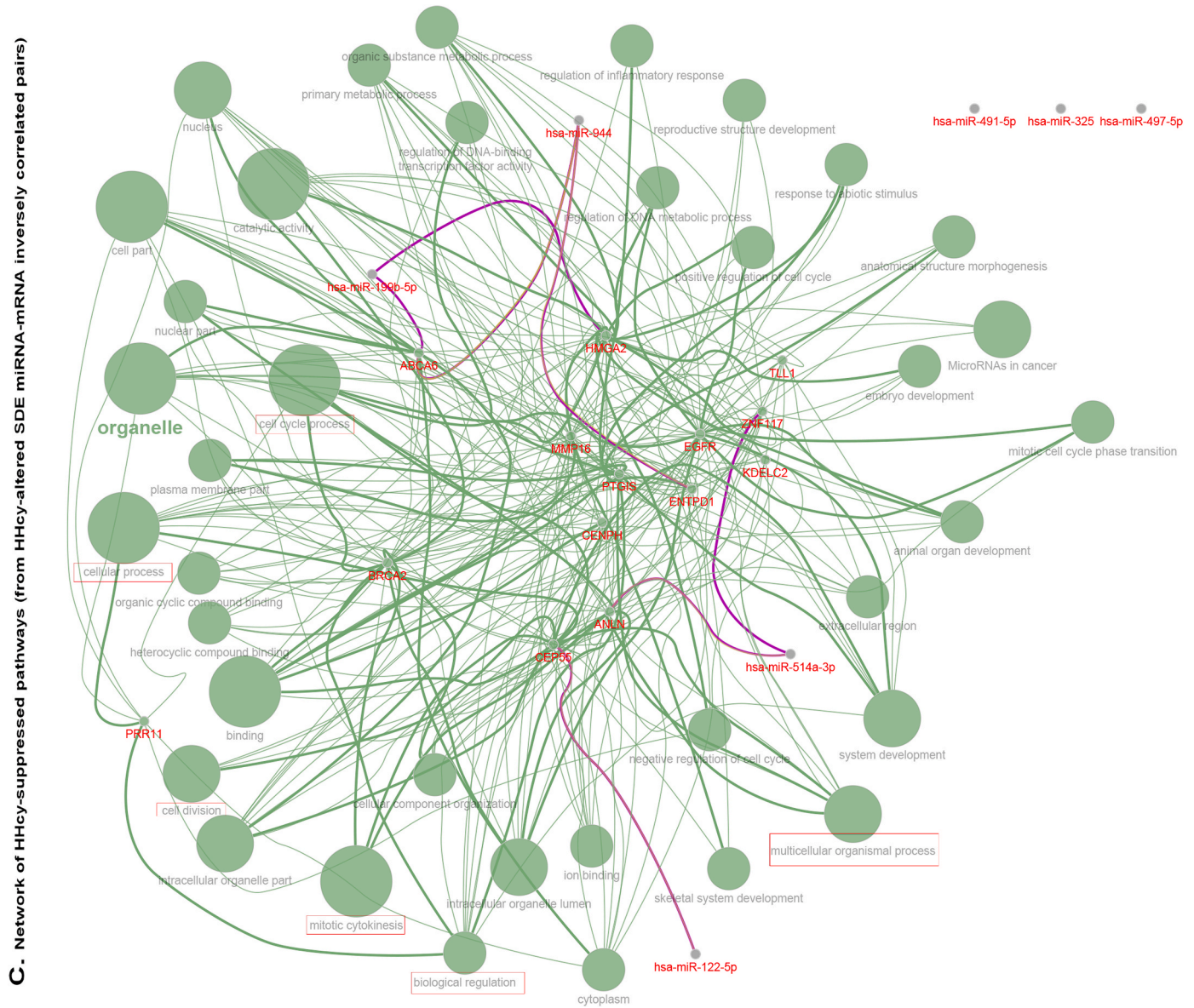


**Fig. 5. Top HHcy-altered pathway network (Cytoscape).** Genes in the top 9 Hcy-altered pathways (FDR<0.05) identified by GSEA (Fig. 2) were further filtered ( $P < 0.05$ ) and visualized using ClueGo v2.5.4 and CluePedia v1.5.4 applications in Cytoscape v3.7.1. to develop the pathway networks. A. Top 4 HHcy-activated pathways and network (from HHcy-induced genes, FDR<0.05). B. Top 5 HHcy-suppressed pathways and network (from HHcy-reduced genes, FDR<0.05). C. Network of HHcy-altered pathways (from HHcy-altered SDE mRNAs,  $P < 0.05$ ,  $FC \geq 1.50$ ). Representative pathways were also found in the top list. Spheres depict pathways in red for suppressed and blue for activated pathways. Small dots with red labeling are representative genes. The color of the dots indicating reduced (red)

and induced (blue) genes. Sphere size proportionally reflects strength of association to the pathway with SDE genes. Thicker network edges represent stronger associations. Pathways are denoted by the colored coded pie. Circled clusters represent matched pathways from A&B to C indicated by color. The names and the statistical details for HHcy-changed and the HHcy-altered SDE mRNA are listed in [Supplementary Tables 1 and 2](#) Abbreviations: FDR, false discovery rate; HHcy, hyperhomocysteinemia; mRNA, messenger RNA; SDE, significantly differentially expressed. (For interpretation of the references to color in this figure legend, the reader is referred to the Web version of this article.)



**D. Network of 4 HHcy-suppressed pathways (from HHcy-altered SDE miRNA-mRNA inversely correlated pairs)**

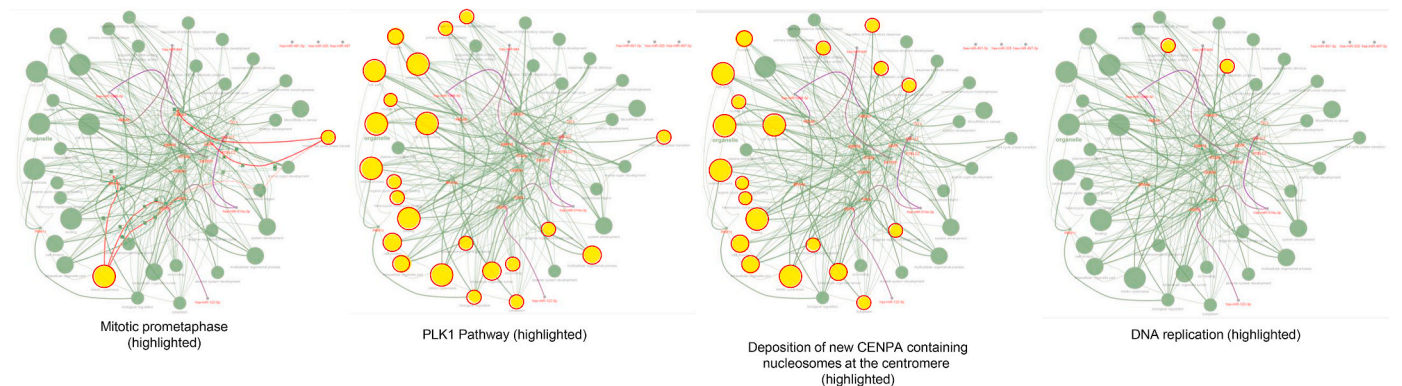


**Fig. 5. (continued).**



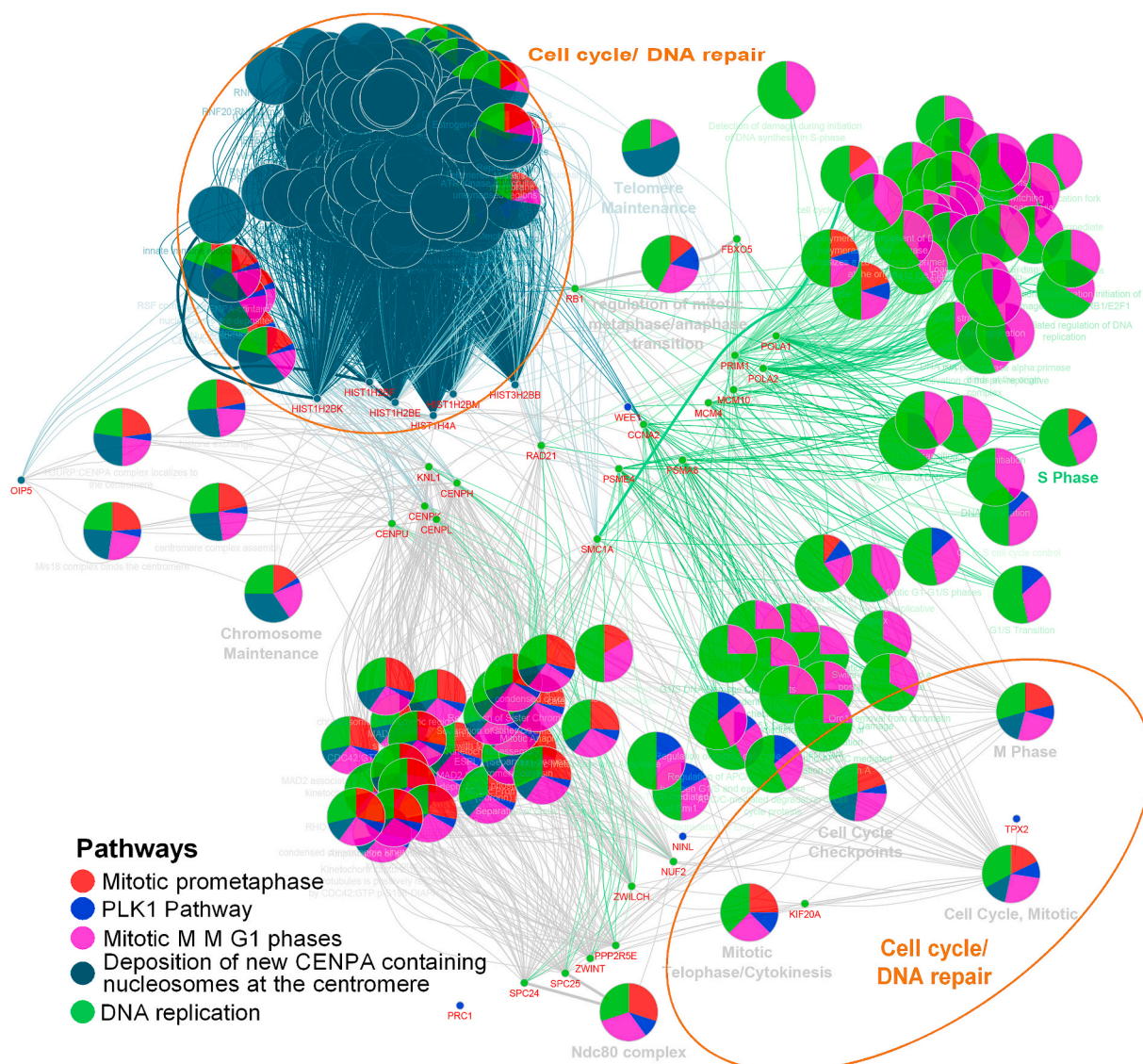


Fig. 6. (continued).

oxaloacetate and pyruvate dehydrogenase E1 subunit alpha 1 (PDHA1), which converts pyruvate to acetyl-CoA, respectively. Acetyl-CoA provides a link to the TCA cycle. HHcy induced glutamic-oxaloacetic transaminase 1/2 (GOT1/2) and malate dehydrogenase 1/2 (MDH1/2), which facilitates aspartate and malate metabolism.

Fatty acid  $\beta$ -oxidation process (Supplementary Fig. 1B). HHcy induced expression of acyl-CoA synthetase long-chain family member 5 (ACSL5), which catalyzes the conversion of long-chain FAs to their active form acyl-CoA; carnitine palmitoyltransferase 2 (CPT2), which oxidizes long-chain FAs in the mitochondria; and solute carrier family 25 member 20 (SLC25A20), which mediates the transport of acylcarnitines into the mitochondrial matrix. HHcy also induced acyl-CoA dehydrogenase long-chain (ACADL), which catalyzes the initial step of mitochondrial  $\beta$ -oxidation of straight-chain FA; enoyl-CoA hydratase; short-chain 1 (ECHS1), which catalyzes the second step of the mitochondrial FA  $\beta$ -oxidation; and hydroxyacyl-CoA dehydrogenase trifunctional multienzyme complex subunit beta (HADHB), which catalyzes the last three steps of mitochondrial  $\beta$ -oxidation of long-chain FAs. In contrast, HHcy reduced expression of carnitine O-acetyltransferase (CRAT), which transports FAs (short-chain FAs) for  $\beta$ -oxidation.

Glutamate metabolic process (Supplementary Fig. 1C). HHcy

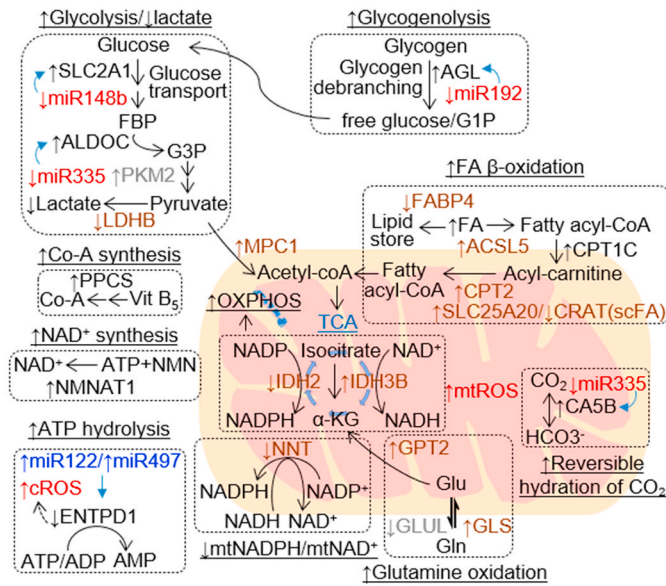
induced expression of glutaminase (GLS), which catalyzes the conversion of glutamine to glutamate and glutamic-pyruvic transaminase 2 (GPT2), which catalyzes the reversible transamination between alanine and 2-oxoglutarate to form pyruvate and glutamate. In contrast, HHcy reduced the expression of glutamate-ammonia ligase (GLUL), glutamate dehydrogenase 1 (GLUD1), and glutamate-cysteine ligase modifier subunit (GCLM).

TCA cycle (Supplementary Fig. 1D). HHcy induced expression of most genes including aconitase 2 (ACO2), isocitrate dehydrogenase (NAD(+) 3 non-catalytic subunit beta (IDH3B), oxoglutarate dehydrogenase (OGDH), succinate-CoA ligase GDP/ADP-forming subunit alpha/beta (SUCLG1/2/A2), succinate dehydrogenase complex subunit C/D (SDHC/D), fumarate hydratase (FH), and malate dehydrogenase 2 (MDH2). In contrast, HHcy reduced the expression of citrate synthase (CS), isocitrate dehydrogenase (NADP(+) 2 (IDH2) and succinate dehydrogenase complex flavoprotein subunit A/B (SDHA/B).

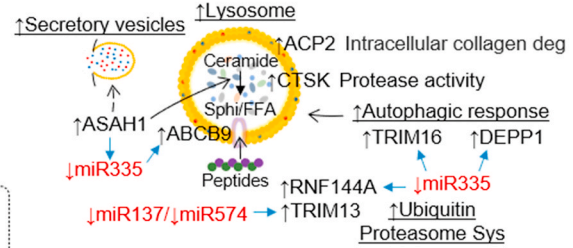
OXPHOS (Supplementary Fig. 1E). HHcy induced the expression of most mitochondrial electron transfer chain (mtETC) complex I genes, including NDUFA2/3/5-9, NDUFB2-4/6-10, NDUFC1/2, NDUFAB1, NDUFS1-6/8, and NDUFV1, but reduced NDUFA1/10, NDUFB1/B5, NDUFS7, and NDUFV2/3. For mt-ETC complex II genes, HHcy induced SDHC/D and reduced SDHA/B. Among mt-ETC complex III genes, HHcy



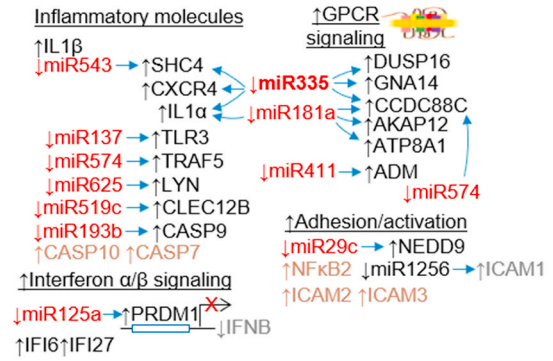
**A. HHcy-activated energy/redox metabolism**



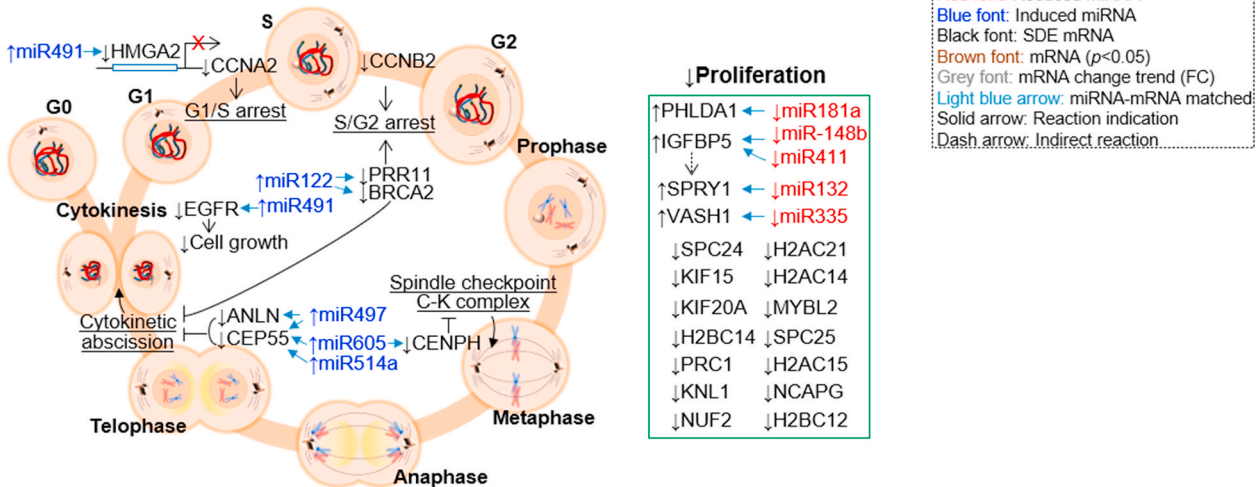
**B. HHcy-activated degradation signaling**



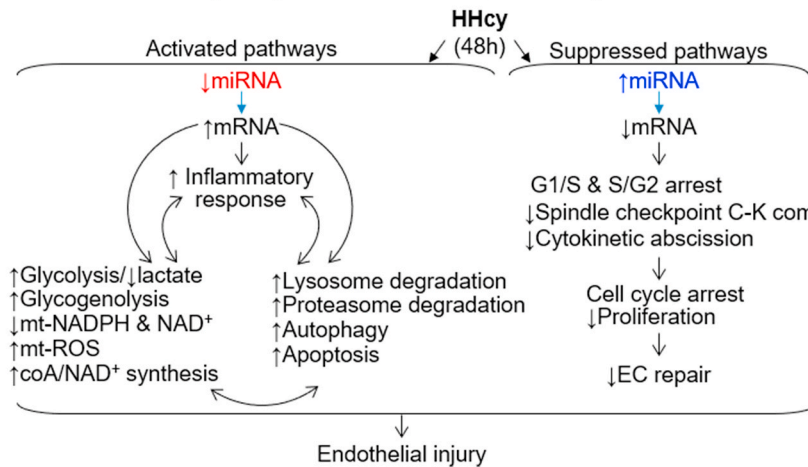
**C. HHcy-activated inflammatory signaling**



**D. HHcy-induced cell cycle arrest and decreased proliferation**



**E. Model of early HHcy molecular and metabolic responses in EC**



(caption on next page)

**Fig. 7. HHcy-altered molecular signaling and associated metabolic processes changes in endothelial cells.** Molecular processes are established based on literature information relevant to the identified HHcy-altered miRNA-matched and non-matched SDE mRNAs (Figs. 5 and 6 and Supplementary File 1). A. Energy/redox metabolism. HHcy alters energy metabolism by increasing glycolysis, glycogenolysis, FA oxidation, glutamine oxidation and NAD/CoA synthesis. In contrast, HHcy decreases mtNADPH/mtNAD<sup>+</sup> which contribute to increased oxidative stress and redox disparity. B. Degradation signaling. HHcy also activates degradation processes including lysosome, autophagy and proteasome, and secretory vesicles. C. Inflammatory signaling. HHcy activates inflammatory response comprised mostly by stimulating pro-inflammatory cytokines and adhesion molecules and in part via GPCR and interferon  $\alpha/\beta$  signaling. D. Cell cycle arrest and decreased proliferation. HHcy arrests cell cycle in various transitions and check points and suppresses proliferation through various axes and mRNA. E. Model of early HHcy molecular and metabolic responses in EC. This hypothetical model summarizes early metabolic, molecular and biological processes identified in HAEC treated with 500  $\mu$ M L-Hcy. Gene symbol details can be seen in [Supplementary Table 1](#). Abbreviations: HHcy, hyperhomocysteinemia; C-K com, centromere-kinetochore complex; Vit, vitamin; Gln, glutamine; Glu, glutamate; deg, degradation; Sys, system; mt, mitochondrial; c, cytosolic; ROS, reactive oxygen species; G1P, glucose 1 phosphate; FA, fatty acid; GPCR, g protein-coupled receptor; miRNA, microRNA; mRNA, messenger RNA; SDE, significantly differentially expressed.

glucose uptake and glycolysis are increased by pro-inflammatory cytokines through NF- $\kappa$ B activation in EC under pathological shear stress conditions [21].

Similar to metabolic changes observed in inflammatory EC and immune cells, we found increased glucose uptake and glycolysis in HHcy. However, lactate synthesis signaling, as a general consequence of glycolysis was suppressed. We identified the potential of preferred pyruvate transportation into mitochondria to be converted to acyl-CoA and oxidized through OXPHOS.

HHcy activated glucose uptake and glycolysis, and switched pyruvate metabolism from lactate synthesis to mitochondrial oxidation signaling in EC (Fig. 7A) — We found that HHcy increased glucose uptake signaling through the  $\downarrow$ miR148b $\rightarrow$  $\uparrow$ SLC2A axis in EC, which facilitates glucose transportation into the cell. In addition, HHcy activated glycolysis signaling through the  $\downarrow$ miR335 $\rightarrow$  $\uparrow$ ALDOC axis. ALDOC is a key glycolytic enzyme that catalyzes the conversion of fructose-1,6BP to glyceraldehyde 3P. We also observed the trend of increased expression of other glycolytic enzymes (Supplementary Fig. 1A). Consistent with our findings,  $\downarrow$ miR148b $\rightarrow$  $\uparrow$ SLC2A signal change was found responsible for increased glycolysis and lactate in gastric cancer [44]. In addition, we observed an overwhelming trend toward suppression of lactate synthesis signaling shown by the reduced expression of lactate dehydrogenase (LDH), especially LDHB which converts pyruvate to lactate. Pyruvate, NADH, and ATP are the byproducts of glycolysis. Pyruvate could be reduced to lactate, be utilized for alanine synthesis, or be transported to the mitochondrial to be oxidized through the TCA cycle and OXPHOS [45]. In addition, glycolysis can branch to the pentose phosphate pathway (PPP) and hexosamine biosynthetic pathway (HBP) [45]. Cardiomyocytes increase glycolysis in hypertrophic remodeling and heart failure [45]. Increased glycolysis is also observed in tumor cells, which leads to lactate accumulation that supports tumor growth and immune resistance [46]. Increased glycolysis and lactate production were observed in HUVEC exposed to pathogenic shear stress along with increased inflammation response [47]. Elevated glycolysis rates maintained lactate production, which is considered as pro-angiogenic signaling in EC [22]. However, LDH inhibition reduced HUVEC tube formation in the presence of L-lactate [48].

Taken together, our findings support the notion that HHcy promotes glucose oxidation through increasing glycolysis, suppressing lactate synthesis, and increasing pyruvate transportation into mitochondria to be oxidized through TCA and OXPHOS, which may contribute to suppressed EC proliferation and angiogenesis.

HHcy activated glycogenolysis signaling (Fig. 7A) — We found that HHcy increased glycogenolysis through the  $\downarrow$ miR 192- $\uparrow$ AGL axis. Amylo-alpha-1,6-glycosidase, 4-alpha-glucanotransferase (AGL) is a glycogen debranching enzyme that breaks down glycogen to glucose 1-phosphate and free glucose. EC can store glycogen from glucose, which may be used as an energy reserve to support glucose production when the supply is restricted or when glycolysis is dysfunctional [49]. Our findings suggest that HHcy-activated glycolysis would increase glucose utilization, therefore activating glycogenolysis to supply additional glucose to increase energy demand.

HHcy activated FA  $\beta$ -oxidation signaling — We found a trend of HHcy-increased FA  $\beta$ -oxidation signaling favoring the long-chain FA

$\beta$ -oxidation (Supplementary Fig. 1B). This impression is supported by the trend of increased expression of long-chain FA  $\beta$ -oxidation signaling genes SLC25A20, ACSL5 and CPT2, and reduced expression of short-chain FA  $\beta$ -oxidation gene CRAT and fatty acid binding protein 4 (FABP4). SLC25A20 transports long-chain FA acylcarnitine into the mitochondrial matrix. Knockdown of FABP4 was associated with increase FA  $\beta$ -oxidation and ROS production [22,50]. FA  $\beta$ -oxidation generates acyl-CoA which fuels the TCA cycle. Taken together, HHcy-increased FA  $\beta$ -oxidation to compensate for the increased energy demand due to glucose limitation, similar as in increased glycogenolysis. However, these metabolic changes increased the risk of oxidative injury in EC.

HHcy activated glutamine oxidation signaling — Glutamine oxidation can fuel the TCA cycle by firstly being converted to glutamate and then becoming 2-oxoglutarate, also termed as  $\alpha$ -ketoglutarate ( $\alpha$ -KG), an intermediate metabolite of the TCA cycle [49]. We found the trend of increased of glutamate generation signaling (Supplementary Fig. 1C) in Hcy-treated EC as glutaminase (GLS) expression is increased, which catalyzes the conversion of glutamine to glutamate, and GLUL expression is decreased, which facilitates the conversion of glutamate to glutamine. This increased glutamate generation most likely fuels the TCA cycle as GPT2 expression is elevated, which catalyzes the transamination from glutamate to 2-oxoglutarate ( $\alpha$ -ketoglutarate) [51]. Our finding supports the notion that HHcy increases glutamine oxidation signaling to supply the TCA cycle (Supplementary Fig. 1D). This is supported by previous evidence showing that limited glucose availability increases glutamine oxidation to cope with ATP demands [49].

HHcy increases OXPHOS activity mt/cROS production in early response — Homeostatic redox regulation is crucial to maintain ROS production at physiological levels, which is essential for cellular function and survival. Redox balance assures that the cell responds properly to insults under pathophysiological conditions. Here, we identified 4 potential mechanisms that contribute to HHcy-induced redox imbalances in EC.

Firstly, HHcy may elevate mtROS generation by promoting the TCA cycle and OXPHOS (Supplementary Figs. 1D and E) due to activated glucose, FA and glutamine oxidation in the early response of EC, a condition similar to the EC treatment conditions in this study (48 h treatment). This early response might lead to a chronic condition, as we reported via database mining, in which HHcy suppresses mt-ETC complex I genes leading to impaired electron transfer cascade and disruption of redox homeostasis [29]. Secondly, HHcy may promote mtROS production though the  $\downarrow$ miR335 $\rightarrow$  $\uparrow$ CA5B axis, as carbonic anhydrase 5B (CA5B) induction was associated with increased mtROS production in mouse cerebral pericytes [52]. Thirdly, HHcy may impair mtROS clearance by suppressing nicotinamide nucleotide transhydrogenase (NNT)/IDH2-related mtNADPH/mtNAD<sup>+</sup> production, as NNT and IDH2 are responsible for the maintenance of NADP<sup>+</sup>/NADPH and NAD<sup>+</sup>/NADH balance in mitochondria [53,54]. This may explain the increased NAD<sup>+</sup> synthesis via nicotinamide nucleotide adenyllyl-transferase 1 (NMNAT1) induction to compensate for cellular needs. A sufficient mtNADPH/mtNAD<sup>+</sup> pool is essential for glutathione formation, which is responsible for the clearance of mtROS (hydrogen peroxide) generated from OXPHOS. Fourthly, HHcy may increase cROS

production by the  $\uparrow$ miR 122/ $\uparrow$ miR497 $\rightarrow$  $\downarrow$ ENTPD1 axis. This is supported by the association of ENTPD1 reduction with suppressed ROS clearance in porcine EC [55].

Taken together, our above findings support the hypothesis that HHcy promotes mt/cROS production by OXPHOS activation and the  $\downarrow$ miR335 $\rightarrow$  $\uparrow$ CA5B axis, and impairs mt/cROS clearance by suppressing NNT/IDH2-related mt-NADPH/mt-NAD<sup>+</sup> production and by reducing ectonucleoside triphosphate diphosphohydrolase 1 (ENTPD1) in the early response. These may contribute to increased endothelial injury and atherosclerosis in HHcy.

HHcy activated degradation processes signaling in EC (Fig. 7B) — Lysosomes and proteasomes are the key mediators of cellular protein degradation. Lysosomes degrade macromolecules. The autophagy process delivers cytoplasmic components and organelles to lysosomes for degradation. In contrast, proteasomes degrade specific single proteins via the ubiquitin-proteasome system (UPS). We identified that HHcy induced the  $\downarrow$ miRNA335 $\rightarrow$  $\uparrow$ ASAH1/ $\uparrow$ ABCB9 molecular axes, both of which are involved in lysosomal degradation. N-Acylsphingosine amidohydrolase 1 (ASAH1) is a member of the acid ceramidase family, which hydrolyses the toxic ceramides to sphingosine and free FA [56]. ATP binding cassette subfamily B member 9 (ABCB9) is a member of the superfamily of ATP-binding cassette (ABC) transporters, which translocate peptides from the cytosol to the lysosomal lumen for degradation [57]. In addition, we also found that HHcy induced the expression of cathepsin K (CTSK) and acid phosphatase 2, lysosomal (ACP2). CTSK is a lysosomal cysteine proteinase (cathepsin) involved in the protein turnover process and was induced in arterial walls showing inflammation and degradation of elastin and collagen [58]. ACP2 is a lysosomal membrane protein and a member of histidine acid phosphatase family that hydrolyzes orthophosphoric monoesters to alcohol and phosphate and plays a critical role in mannose-6-phosphate removal. ACP2 is also essential in cerebellar development and its mutation causes severe cerebellar neurodevelopmental and neurodegenerative disorders [59].

Taken together, our findings suggest that HHcy may activate lysosomal process for protein, ceramide and mannose-6-phosphate degradation via ASAH1, ABCB9, CTSK and ACP2 induction, which facilitate HHcy-induced lysosomal dysfunction in EC. We previously suggested that Hcy action in EC is dependent on intact lysosomal function, as lysosomal inhibitor monensin and concanamycin A suppressed Hcy uptake in HAEC but not in human vascular smooth muscle cells (HVMSC) [14]. Lysosomal activation is likely a compensatory or pathologically relevant process in HHcy-induced endothelial injury.

HHcy activated inflammatory signaling in EC (Fig. 7C) — ECs can be activated by the upregulation of adhesion molecules such as E-selectin, ICAM-1, and VCAM-1 which allow immune cells to adhere and cause tissue inflammation. We identified the  $\downarrow$ miR29c $\rightarrow$  $\uparrow$ NEDD9 and the  $\downarrow$ miR1256 $\rightarrow$  $\uparrow$ ICAM-1 axes in HHcy EC. Neural precursor cell expressed, developmentally down-regulated 9 (NEDD9) is a focal adhesion protein acting as a scaffold to regulate signaling complexes for cell migration. Increased expression of NEDD9 has been linked to fibrotic vascular remodeling and pulmonary hypertension in animal models [60]. ICAM-1 is an adhesion molecule that can be induced in different proinflammatory conditions through an NF $\kappa$ B-dependent transactivation mechanism [61–63]. It is known that increased ICAM-1 mediates tissue inflammation by facilitating leukocyte infiltration [64]. We found that HHcy increased ICAM-1 by 1.5-fold ( $p = 0.054$ ). Our evidence suggested that HHcy may activate EC and promote tissue inflammation by the  $\downarrow$ miR29c $\rightarrow$  $\uparrow$ NEDD9 and the  $\downarrow$ miR1256 $\rightarrow$  $\uparrow$ ICAM1 axes.

Our data also suggested that HHcy may promote tissue inflammation by activating inflammasomes and inducing pyroptosis, a well-established inflammatory cell death pathway. We found that HHcy induced the expression of inflammasome/pyroptosis-related signaling such as the  $\downarrow$ miR137 $\rightarrow$  $\uparrow$ toll like receptor 3 (TLR3), the  $\downarrow$ miR574 $\rightarrow$  $\uparrow$ TNF receptor associated factor 5 (TRAF5) and the  $\downarrow$ miR193b $\rightarrow$  $\uparrow$ caspase (CASP)-9 axes, and inflammasome activation products interleukin 1

alpha/beta (IL1 $\alpha$ / $\beta$ ) and CASP-10/7. These are consistent with our previous findings that HHcy induces EC pyroptosis by CASP-1 activation/mitochondrial dysfunction/CASP-9/3 activation and increases vessel wall inflammation in type II diabetes mellitus [65].

GPCRs are membrane receptors that respond to a variety of external signals and interact with G proteins that bind to GTP or GDP and in turn trigger a large range of signaling from growth to hormone and inflammatory responses [66,67]. We found that HHcy induced the expression of some inflammation-related GPCR proteins, such as C-X-C motif chemokine receptor 4 (CXCR4) and G protein  $\alpha$  subunit 14 (GNA14), including their miRNA axes ( $\downarrow$ miRNA335 $\rightarrow$  $\uparrow$ CXCR4/ $\uparrow$ GNA14). CXCR4 is a GPCR chemokine receptor that plays crucial role in leukocyte recruitment. CXCR4 can bind to LPS and activate MAPK1/3 and AKT signaling [68–71]. GNA14 is a member of G $\alpha$ q/11 subfamily which mediates EC migration and permeability in response to FGF2 and VEGFA, potentially by phospholipase C- $\beta$ 3 activation [72]. GNA14 is involved in hypertensive diseases and tumor vascularization [72]. The induction of CXCR4 and GNA14 signaling in Hcy-treated EC implicates their contribution to leukocyte infiltration and vascular leakage in HHcy-related tissue inflammation and vascular disease.

HHcy suppressed cell cycle and proliferation signaling in EC (Fig. 7D) — We previously reported that HHcy arrests the cell cycle at the G1/S transition by cyclin A transcriptional suppression via DNA hypomethylation at the CDE suppressor binding site [10]. Here, we identified upstream signaling of cyclin A suppression axes, miR491 $\rightarrow$  $\downarrow$ HMG2 $\rightarrow$  $\downarrow$ CCNA2 (cyclin A)/CCNB2 (cyclin B). The high mobility group protein AT-hook 2 (HMG2) is a transcriptional factor binding to consensus sequences 5'-ATATTGCGCAWWATT-3' and 5'-ATATTGCGCAWWATT-3', where W represents A or T, and is involved in CCNA2 transactivation [73]. Since cyclin B regulates the S/G2 transition, HHcy may also arrest the cell cycle at the S/G2 transition though CCNB2 suppression and the  $\uparrow$ miR22 $\rightarrow$  $\downarrow$ proline rich 11 (PRR11)/ $\downarrow$ BRCA2 DNA repair associated (BRCA2) axes. In addition, HHcy may arrest the cell cycle by disrupting the spindle checkpoint of centromere-kinetochore complex via the  $\uparrow$ miR6045 $\rightarrow$  $\downarrow$ centromere protein H (CENPH) axis and cytokinetic abscission through the miR605/-miR497/miR514a $\rightarrow$ centrosomal protein 55 (CEP55) axes. In addition to cell cycle arrest HHcy may suppress EC proliferation through a few signaling pathways (Fig. 7B), including the  $\downarrow$ miR335 $\rightarrow$  $\uparrow$ VASH1 and the  $\downarrow$ miR181a $\rightarrow$  $\uparrow$ PHLDA1 axes. Vasohibin 1 (VASH1) belongs to the transglutaminase-like cysteine protease superfamily, which is recognized as an angiogenesis inhibitor that also inhibits migration, proliferation, and network formation in HUVEC [74]. Pleckstrin homology-like domain, family A, member 1 (PHLDA1) is member of the pleckstrin homology-related domain protein family, with undefined function. PHLDA1 was found to be induced by Hcy and associated with cell death in human EC [75]. Overexpression of PHLDA1 by transient transfection induced DNA fragmentation corresponding to programmed cell death in HAEC and inhibition of proliferation and migration in breast cancer cells [76].

In accordance with our previous findings, the current study suggests that HHcy may suppress EC cell cycle and proliferation by multiple molecular signaling pathways, including miR491 $\rightarrow$  $\downarrow$ HMG2 $\rightarrow$  $\downarrow$ CCNA2/CCNB2,  $\uparrow$ miR22 $\rightarrow$  $\downarrow$ PRR11/ $\downarrow$ BRCA2, miR6045 $\rightarrow$  $\downarrow$ CENPH, miR605/miR497/miR514a $\rightarrow$ CEP55,  $\downarrow$ miR335 $\rightarrow$  $\uparrow$ VASH1 and  $\downarrow$ miR181a $\rightarrow$  $\uparrow$ PHLDA1.

Several methodological and analytical limitations require acknowledgement. Our high-throughput gene expression profiling analysis provides compelling data for specific miRNA-mRNA signaling and regulatory networks. As all gene expression profiling studies require confirmation and functional validation, biological plausibility was further complemented with additional bioinformatic analyses and literature review. Statistical considerations for multiple simultaneous inferences include conservatively minimizing family-wise error rate (FWER) or more commonly minimizing FDR, which increases statistical power [31]. While our primary microarray analysis relied on

fold-change and associated p-values, additional GSEA presented data for both PWER and FDR. This study examined one timepoint. Considering that changes in miRNA expression might be expected to precede changes in targeted mRNA expression, a single timepoint might not appreciate this time course. This consideration would apply to GSEA as well. Nevertheless, since cells were not synchronized prior to treatment, it is likely that cells were at least in different phases of the cell cycle at time of treatment. GSEA and Cytoscape analysis are limited to their respective databases and the effects of some miRNA and mRNA expression changes might not yet be able to be fully characterized with these tools. Still, this overall study benefits from many strengths described above including physiological relevance, robust evidence from multiple data sources, and novelty.

In conclusion, this study explores the early molecular responses in EC by which HHcy contributes to CVD and suggests a myriad of canonical pathways. This conclusion was reached by unbiased systematic analyses based on HHcy-altered mRNA and miRNA expression changes. We identified potential molecular networks and axes involving HHcy-activated glucose uptake, glycolysis, glycogenolysis, FA  $\beta$ -oxidation, glutamine oxidation, OXPHOS, production of mt/cROS and inflammatory cytokine/adhesion molecules, lysosome/proteasome degradation and inflammasome/pyroptosis processes. We also identified potential molecular axes for HHcy-switched pyruvate metabolism from lactate synthesis to mitochondrial oxidation signaling, and HHcy-suppressed proliferation in EC. Our findings affirm previous observations and contributes a wealth of new knowledge to the field of CVD research. Molecular pathways and biochemical processes identified in this study are useful not only for understanding mechanisms by which HHcy induces CVD, but also for discovering potential therapeutic targets.

## Funding

This work was supported in part by the National Institutes of Health (NIH) grants HL82774, HL-110764, HL130233, HL131460, DK104114, DK113775, and HL131460 to HW.

## Disclosures

MJ is currently employed by Otsuka Pharmaceutical Development & Commercialization, Inc.

## Data availability statement

The data present in the study are deposited in the Gene Expression Omnibus (GEO) repository under the accession number: GEO: GSE175748.

## Declaration of competing interest

The authors declare that they have no conflict of interest with respect to this manuscript.

## Appendix A. Supplementary data

Supplementary data to this article can be found online at <https://doi.org/10.1016/j.redox.2021.102018>.

## Abbreviations

Ade	adenosine
CVD	cardiovascular disease
EC	endothelial cell
FDR	false discovery rate
HAEC	human aortic endothelial cell
Hcy	homocysteine
miRNA	microRNA

mRNA messenger RNA  
SDE significantly differentially expressed

## References

- [1] M.E. Lee, H. Wang, Homocysteine and hypomethylation. A novel link to vascular disease, *Trends Cardiovasc. Med.* 9 (1999) 49–54.
- [2] R. Obeid, W. Herrmann, Mechanisms of homocysteine neurotoxicity in neurodegenerative diseases with special reference to dementia, *FEBS Lett.* 580 (2006) 2994–3005.
- [3] B.A. Maron, J. Loscalzo, The treatment of hyperhomocysteinemia, *Annu. Rev. Med.* 60 (2009) 39–54.
- [4] P. Fang, D. Zhang, Z. Cheng, C. Yan, X. Jiang, W.D. Kruger, S. Meng, E. Arning, T. Bottiglieri, E.T. Choi, Y. Han, X.F. Yang, H. Wang, Hyperhomocysteinemia potentiates hyperglycemia-induced inflammatory monocyte differentiation and atherosclerosis, *Diabetes* 63 (2014) 4275–4290.
- [5] Z. Cheng, X. Jiang, M. Pansuria, P. Fang, J. Mai, K. Mallilankaraman, R. K. Gandhirajan, S. Eguchi, R. Scalia, M. Madesh, X. Yang, H. Wang, Hyperhomocysteinemia and hyperglycemia induce and potentiate endothelial dysfunction via mu-calpain activation, *Diabetes* 64 (2015) 947–959.
- [6] Y. Huo, J. Li, X. Qin, Y. Huang, X. Wang, R.F. Gottesman, G. Tang, B. Wang, D. Chen, M. He, J. Fu, Y. Cai, X. Shi, Y. Zhang, Y. Cui, N. Sun, X. Li, X. Cheng, J. Wang, X. Yang, T. Yang, C. Xiao, G. Zhao, Q. Dong, D. Zhu, X. Wang, J. Ge, L. Zhao, D. Hu, L. Liu, F.F. Hou, C. Investigators, Efficacy of folic acid therapy in primary prevention of stroke among adults with hypertension in China: the CSPPT randomized clinical trial, *J. Am. Med. Assoc.* 313 (2015) 1325–1335.
- [7] D. Xie, Y. Yuan, J. Guo, S. Yang, X. Xu, Q. Wang, Y. Li, X. Qin, G. Tang, Y. Huo, G. Deng, S. Wu, B. Wang, Q. Zhang, X. Wang, P. Fang, H. Wang, X. Xu, F. Hou, Hyperhomocysteinemia predicts renal function decline: a prospective study in hypertensive adults, *Sci. Rep.* 5 (2015) 16268.
- [8] M.A. Gimbrone Jr., G. Garcia-Cardena, Endothelial cell dysfunction and the pathobiology of atherosclerosis, *Circ. Res.* 118 (2016) 620–636.
- [9] H. Wang, M. Yoshizumi, K. Lai, J.C. Tsai, M.A. Perrella, E. Haber, M.E. Lee, Inhibition of growth and p21ras methylation in vascular endothelial cells by homocysteine but not cysteine, *J. Biol. Chem.* 272 (1997) 25380–25385.
- [10] M.D. Jamaluddin, I. Chen, F. Yang, X. Jiang, M. Jan, X. Liu, A.I. Schafer, W. Durante, X. Yang, H. Wang, Homocysteine inhibits endothelial cell growth via DNA hypomethylation of the cyclin A gene, *Blood* 110 (2007) 3648–3655.
- [11] J. Nelson, Y. Wu, X. Jiang, R. Berretta, S. Houser, E. Choi, J. Wang, J. Huang, X. Yang, H. Wang, Hyperhomocysteinemia suppresses bone marrow CD34+/VEGF receptor 2+ cells and inhibits progenitor cell mobilization and homing to injured vasculature—a role of beta1-integrin in progenitor cell migration and adhesion, *Faseb. J.* 29 (2015) 3085–3099.
- [12] P.Y. Chang, S.C. Lu, C.M. Lee, Y.J. Chen, T.A. Dugan, W.H. Huang, S.F. Chang, W. S. Liao, C.H. Chen, Y.T. Lee, Homocysteine inhibits arterial endothelial cell growth through transcriptional downregulation of fibroblast growth factor-2 involving G protein and DNA methylation, *Circ. Res.* 102 (2008) 933–941.
- [13] H.P. Zhang, Y.H. Wang, S.C. Ma, H. Zhang, A.N. Yang, X.L. Yang, M.H. Zhang, J. M. Sun, Y.J. Hao, Y.D. Jiang, Homocysteine inhibits endothelial progenitor cells proliferation via DNMT1-mediated hypomethylation of Cyclin A, *Exp. Cell Res.* 362 (2018) 217–226.
- [14] X. Jiang, F. Yang, E. Brailoiu, H. Jakubowski, N.J. Dun, A.I. Schafer, X. Yang, W. Durante, H. Wang, Differential regulation of homocysteine transport in vascular endothelial and smooth muscle cells, *Arterioscler. Thromb. Vasc. Biol.* 27 (2007) 1976–1983.
- [15] S. Dayal, I.O. Blokhin, R.A. Erger, M. Jensen, E. Arning, J.W. Stevens, T. Bottiglieri, F.M. Faraci, S.R. Lentz, Protective vascular and cardiac effects of inducible nitric oxide synthase in mice with hyperhomocysteinemia, *PLoS One* 9 (2014), e107734.
- [16] J.K. Liao, Linking endothelial dysfunction with endothelial cell activation, *J. Clin. Invest.* 123 (2013) 540–541.
- [17] M.D. Silverman, R.J. Tumuluri, M. Davis, G. Lopez, J.T. Rosenbaum, P.I. Lelkes, Homocysteine upregulates vascular cell adhesion molecule-1 expression in cultured human aortic endothelial cells and enhances monocyte adhesion, *Arterioscler. Thromb. Vasc. Biol.* 22 (2002) 587–592.
- [18] M. Barroso, D. Kao, H.J. Blom, I. Tavares de Almeida, R. Castro, J. Loscalzo, D. E. Handy, S-adenosylhomocysteine induces inflammation through NFkB: a possible role for EZH2 in endothelial cell activation, *Biochim. Biophys. Acta* 1862 (2016) 82–92.
- [19] H. Xi, Y. Zhang, Y. Xu, W.Y. Yang, X. Jiang, X. Sha, X. Cheng, J. Wang, X. Qin, J. Yu, Y. Ji, X. Yang, H. Wang, Caspase-1 inflammasome activation mediates homocysteine-induced pyroptosis in endothelial cells, *Circ. Res.* 118 (2016) 1525–1539.
- [20] Y.P. Leng, Y.S. Ma, X.G. Li, R.F. Chen, P.Y. Zeng, X.H. Li, C.F. Qiu, Y.P. Li, Z. Zhang, A.F. Chen, l-Homocysteine-induced cathepsin V mediates the vascular endothelial inflammation in hyperhomocysteinemia, *Br. J. Pharmacol.* 175 (2018) 1157–1172.
- [21] K. Theodorou, R.A. Boon, Endothelial cell metabolism in atherosclerosis, *Front Cell Dev Biol* 6 (2018) 82.
- [22] G. Eelen, P. de Zeeuw, L. Treps, U. Harjes, B.W. Wong, P. Carmeliet, Endothelial cell metabolism, *Physiol. Rev.* 98 (2018) 3–58.
- [23] G. Fitzgerald, I. Soro-Arnaiz, K. De Bock, The warburg effect in endothelial cells and its potential as an anti-angiogenic target in cancer, *Front Cell Dev Biol* 6 (2018) 100.

- [24] L. Zhang, X. Wang, R. Cueto, C. Effi, Y. Zhang, H. Tan, X. Qin, Y. Ji, X. Yang, H. Wang, Biochemical basis and metabolic interplay of redox regulation, *Redox Biol* 26 (2019) 101284.
- [25] D. Trachootham, W. Lu, M.A. Ogasawara, R.D. Nilsa, P. Huang, Redox regulation of cell survival, *Antioxidants Redox Signal*. 10 (2008) 1343–1374.
- [26] Z. Cheng, X. Yang, H. Wang, Hyperhomocysteinemia and endothelial dysfunction, *Curr. Hypertens. Rev.* 5 (2009) 158–165.
- [27] X. Wu, L. Zhang, Y. Miao, J. Yang, X. Wang, C.C. Wang, J. Feng, L. Wang, Homocysteine causes vascular endothelial dysfunction by disrupting endoplasmic reticulum redox homeostasis, *Redox Biol* 20 (2019) 46–59.
- [28] W. Shen, C. Gao, R. Cueto, L. Liu, H. Fu, Y. Shao, W.Y. Yang, P. Fang, E.T. Choi, Q. Wu, X. Yang, H. Wang, Homocysteine-methionine cycle is a metabolic sensor system controlling methylation-regulated pathological signaling, *Redox Biol* 28 (2020) 101322.
- [29] R. Cueto, L. Zhang, H.M. Shan, X. Huang, X. Li, Y.F. Li, J. Lopez, W.Y. Yang, M. Lavallee, C. Yu, Y. Ji, X. Yang, H. Wang, Identification of homocysteine-suppressive mitochondrial ETC complex genes and tissue expression profile - novel hypothesis establishment, *Redox Biol* 17 (2018) 70–88.
- [30] H. Skovierova, E. Vidomanova, S. Mahmood, J. Sopkova, A. Drgova, T. Cervenova, E. Halasova, J. Lehotsky, The molecular and cellular effect of homocysteine metabolism imbalance on human Health, *Int. J. Mol. Sci.* 17 (2016).
- [31] Y. Benjamini, Y. Hochberg, Controlling the false discovery rate: a practical and powerful approach to multiple testing, *J. Roy. Stat. Soc. B* 57 (1995) 289–300.
- [32] R. Team, RStudio: Integrated Development Environment for R, 456 Ed., 1.1, 2020 (Boston, MA).
- [33] C.H. Chou, S. Shrestha, C.D. Yang, N.W. Chang, Y.L. Lin, K.W. Liao, W.C. Huang, T. H. Sun, S.J. Tu, W.H. Lee, M.Y. Chiew, C.S. Tai, T.Y. Wei, T.R. Tsai, H.T. Huang, C. Y. Wang, H.Y. Wu, S.Y. Ho, P.R. Chen, C.H. Chuang, P.J. Hsieh, Y.S. Wu, W. L. Chen, M.J. Li, Y.C. Wu, X.Y. Huang, F.L. Ng, W. Buddhakosai, P.C. Huang, K. C. Lan, C.Y. Huang, S.L. Weng, Y.N. Cheng, C. Liang, W.L. Hsu, H.D. Huang, miRTarBase update 2018: a resource for experimentally validated microRNA-target interactions, *Nucleic Acids Res.* 46 (2018) D296–D302.
- [34] A. Subramanian, P. Tamayo, V.K. Mootha, S. Mukherjee, B.L. Ebert, M.A. Gillette, A. Paulovich, S.L. Pomeroy, T.R. Golub, E.S. Lander, J.P. Mesirov, Gene set enrichment analysis: a knowledge-based approach for interpreting genome-wide expression profiles, *Proc. Natl. Acad. Sci. U. S. A.* 102 (2005) 15545–15550.
- [35] P. Shannon, A. Markiel, O. Ozier, N.S. Baliga, J.T. Wang, D. Ramage, N. Amin, B. Schwikowski, T. Ideker, Cytoscape: a software environment for integrated models of biomolecular interaction networks, *Genome Res.* 13 (2003) 2498–2504.
- [36] G. Bindea, B. Mlecnik, H. Hackl, P. Charoentong, M. Tosolini, A. Kirilovsky, W. H. Fridman, F. Pages, Z. Trajanoski, J. Galon, ClueGO: a Cytoscape plug-in to decipher functionally grouped gene ontology and pathway annotation networks, *Bioinformatics* 25 (2009) 1091–1093.
- [37] G. Bindea, J. Galon, B. Mlecnik, CluePedia Cytoscape plugin: pathway insights using integrated experimental and in silico data, *Bioinformatics* 29 (2013) 661–663.
- [38] M. Kutmon, S. Lotia, C.T. Evelo, A.R. Pico, WikiPathways App for Cytoscape: making biological pathways amenable to network analysis and visualization, *F1000Res* 3 (2014) 152.
- [39] C. Catalanotto, C. Cogoni, G. Zardo, MicroRNA in control of gene expression: an overview of nuclear functions, *Int. J. Mol. Sci.* 17 (2016).
- [40] S.K. Ray, Neuroblastoma : Molecular Mechanisms and Therapeutic Interventions, 2019.
- [41] J. Dan Dunn, L.A. Alvarez, X. Zhang, T. Soldati, Reactive oxygen species and mitochondria: a nexus of cellular homeostasis, *Redox Biol* 6 (2015) 472–485.
- [42] L. Sun, X. Yang, Z. Yuan, H. Wang, Metabolic reprogramming in immune response and tissue inflammation, *Arterioscler. Thromb. Vasc. Biol.* 40 (2020) 1990–2001.
- [43] J. Ritterhoff, R. Tian, Metabolism in cardiomyopathy: every substrate matters, *Cardiovasc. Res.* 113 (2017) 411–421.
- [44] X. Ding, J. Liu, T. Liu, Z. Ma, D. Wen, J. Zhu, miR-148b inhibits glycolysis in gastric cancer through targeting SLC2A1, *Cancer Med* 6 (2017) 1301–1310.
- [45] D.H. Tran, Z.V. Wang, Glucose metabolism in cardiac hypertrophy and heart failure, *J Am Heart Assoc* 8 (2019), e012673.
- [46] T. Cascone, J.A. McKenzie, R.M. Mbofung, S. Punt, Z. Wang, C. Xu, L.J. Williams, Z. Wang, C.A. Bristow, A. Carugo, M.D. Peoples, L. Li, T. Karpinets, L. Huang, S. Malu, C. Creasy, S.E. Leahy, J. Chen, Y. Chen, H. Pelicano, C. Bernatchez, Y.N. V. Gopal, T.P. Heffernan, J. Hu, J. Wang, R.N. Amaria, L.A. Garraway, P. Huang, P. Yang, I.I. Wistuba, S.E. Woodman, J. Roszik, R.E. Davis, M.A. Davies, J. V. Heymach, P. Hwu, W. Peng, Increased tumor glycolysis characterizes immune resistance to adoptive T cell therapy, *Cell Metabol.* 27 (2018) 977–987, e974.
- [47] Q. Yang, J. Xu, Q. Ma, Z. Liu, V. Sudhahar, Y. Cao, L. Wang, X. Zeng, Y. Zhou, M. Zhang, Y. Xu, Y. Wang, N.L. Weintraub, C. Zhang, T. Fukai, C. Wu, L. Huang, Z. Han, T. Wang, D.J. Fulton, M. Hong, Y. Huo, PRKAA1/AMPKalpha1-driven glycolysis in endothelial cells exposed to disturbed flow protects against atherosclerosis, *Nat. Commun.* 9 (2018) 4667.
- [48] A. Faulkner, E. Lynam, R. Purcell, C. Jones, C. Lopez, M. Board, K.D. Wagner, N. Wagner, C. Carr, C. Wheeler-Jones, Context-dependent regulation of endothelial cell metabolism: differential effects of the PPARbeta/delta agonist GW0742 and VEGF-A, *Sci. Rep.* 10 (2020) 7849.
- [49] D. Verdegem, S. Moens, P. Stapor, P. Carmeliet, Endothelial cell metabolism: parallels and divergences with cancer cell metabolism, *Canc. Metabol.* 2 (2014) 19.
- [50] U. Harjes, E. Bridges, K.M. Gharpure, I. Roxanis, H. Sheldon, F. Miranda, L. S. Mangala, S. Pradeep, G. Lopez-Berestein, A. Ahmed, B. Fielding, A.K. Sood, A. L. Harris, Antiangiogenic and tumour inhibitory effects of downregulating tumour endothelial FABP4, *Oncogene* 36 (2017) 912–921.
- [51] X. Feng, Y. Hao, Z. Wang, Targeting glutamine metabolism in PIK3CA mutant colorectal cancers, *Genes Dis* 3 (2016) 241–243.
- [52] G.N. Shah, T.O. Price, W.A. Banks, Y. Morofuji, A. Kovac, N. Ercal, C.M. Sorenson, E.S. Shin, N. Sheibani, Pharmacological inhibition of mitochondrial carbonic anhydrases protects mouse cerebral pericytes from high glucose-induced oxidative stress and apoptosis, *J. Pharmacol. Exp. Therapeut.* 344 (2013) 637–645.
- [53] J.A. Ronchi, A. Francisco, L.A. Passos, T.R. Figueira, R.F. Castilho, The contribution of nicotinamide nucleotide transhydrogenase to peroxide detoxification is dependent on the respiratory state and counterbalanced by other sources of NADPH in liver mitochondria, *J. Biol. Chem.* 291 (2016) 20173–20187.
- [54] W. Xiao, R.S. Wang, D.E. Handy, J. Loscalzo, NAD(H) and NADP(H) redox couples and cellular energy metabolism, *Antioxidants Redox Signal.* 28 (2018) 251–272.
- [55] E. Chisci, M. De Giorgi, E. Zanfrini, A. Testaseca, E. Brambilla, A. Cinti, L. Farina, B. Kutryb-Zajac, C. Bugarin, C. Villa, E. Grassilli, R. Combi, G. Gaipa, M.G. Cerrito, I. Rivolta, R.T. Smolenski, M. Lavitrano, R. Giovannoni, Simultaneous overexpression of human E5NT and ENTPD1 protects porcine endothelial cells against H2O2-induced oxidative stress and cytotoxicity in vitro, *Free Radic. Biol. Med.* 108 (2017) 320–333.
- [56] C.M. Li, J.H. Park, X. He, B. Levy, F. Chen, K. Arai, D.A. Adler, C.M. Disteche, J. Koch, K. Sandhoff, E.H. Schuchman, The human acid ceramidase gene (ASAH): structure, chromosomal location, mutation analysis, and expression, *Genomics* 62 (1999) 223–231.
- [57] P. Graab, C. Bock, K. Weiss, A. Hirth, N. Koller, M. Braner, J. Jung, F. Loehr, R. Tampe, C. Behrends, R. Abele, Lysosomal targeting of the ABC transporter TAPL is determined by membrane-localized charged residues, *J. Biol. Chem.* 294 (2019) 7308–7323.
- [58] S.P. Lutgens, K.B. Cleutjens, M.J. Daemen, S. Heeneman, Cathepsin cysteine proteases in cardiovascular disease, *Faseb. J.* 21 (2007) 3029–3041.
- [59] N. Ashtari, X. Jiao, M. Rahimi-Balaei, S. Amiri, S.E. Mehr, B. Yeganeh, H. Marzban, Lysosomal acid phosphatase biosynthesis and dysfunction: a Mini review focused on lysosomal enzyme dysfunction in brain, *Curr. Mol. Med.* 16 (2016) 439–446.
- [60] A.O. Samokhin, T. Stephens, B.M. Wertheim, R.S. Wang, S.O. Vargas, L.M. Yung, M. Cao, M. Brown, E. Arons, P.B. Dieffenbach, J.G. Fewell, M. Matar, F.P. Bowman, K.J. Haley, G.A. Alba, S.M. Marino, R. Kumar, I.O. Rosas, A.B. Waxman, W. M. Oldham, D. Khanna, B.B. Graham, S. Seo, V.N. Gladyshev, P.B. Yu, L. E. Fredenburgh, J. Loscalzo, J.A. Leopold, B.A. Maron, NEDD9 targets COL3A1 to promote endothelial fibrosis and pulmonary arterial hypertension, *Sci. Transl. Med.* 10 (2018).
- [61] N. Hadad, L. Tuval, V. Elgazar-Carmom, R. Levy, R. Levy, Endothelial ICAM-1 protein induction is regulated by cytosolic phospholipase A2alpha via both NF-kappaB and CREB transcription factors, *J. Immunol.* 186 (2011) 1816–1827.
- [62] B.S. Wung, C.W. Ni, D.L. Wang, ICAM-1 induction by TNFalpha and IL-6 is mediated by distinct pathways via Rac in endothelial cells, *J. Biomed. Sci.* 12 (2005) 91–101.
- [63] P. Melotti, E. Nicolis, A. Tamanini, R. Rolfini, A. Pavirani, G. Cabrini, Activation of NF-kB mediates ICAM-1 induction in respiratory cells exposed to an adenovirus-derived vector, *Gene Ther.* 8 (2001) 1436–1442.
- [64] A. Zahr, P. Alcaide, J. Yang, A. Jones, M. Gregory, N.G. dela Paz, S. Patel-Hett, T. Nevers, A. Koiraal, F.W. Lusinskas, M. Saint-Geniez, B. Ksander, P.A. D'Amore, P. Argueso, Endomucin prevents leukocyte-endothelial cell adhesion and has a critical role under resting and inflammatory conditions, *Nat. Commun.* 7 (2016) 10363.
- [65] P. Fang, X. Li, H. Shan, J.J. Saredy, R. Cueto, J. Xia, X. Jiang, X.F. Yang, H. Wang, Ly6C(+) inflammatory monocyte differentiation partially mediates hyperhomocysteinemia-induced vascular dysfunction in type 2 diabetic db/db mice, *Arterioscler. Thromb. Vasc. Biol.* 39 (2019) 2097–2119.
- [66] C.M.A.J.U. O'Connor, in: C. O'Connor (Ed.), *Essentials of Cell Biology*, NPG Education, Cambridge, MA, 2010.
- [67] L. Sun, R.D. Ye, Role of G protein-coupled receptors in inflammation, *Acta Pharmacol. Sin.* 33 (2012) 342–350.
- [68] T. Lear, S.R. Dunn, A.C. McKelvey, A. Mir, J. Evankovich, B.B. Chen, Y. Liu, RING finger protein 113A regulates C-X-C chemokine receptor type 4 stability and signaling, *Am. J. Physiol. Cell Physiol.* 313 (2017) C584–C592.
- [69] Y. Cao, Z.R. Hunter, X. Liu, L. Xu, G. Yang, J. Chen, C.J. Patterson, N. Tsakmaklis, S. Kanan, S. Rodig, J.J. Castillo, S.P. Treon, The WHIM-like CXCR4(S338X) somatic mutation activates AKT and ERK, and promotes resistance to ibuprofen and other agents used in the treatment of Waldenstrom's Macroglobulinemia, *Leukemia* 29 (2015) 169–176.
- [70] C.T. Veldkamp, C. Seibert, F.C. Peterson, N.B. De la Cruz, J.C. Haugner 3rd, H. Basnet, T.P. Sakmar, B.F. Volkman, Structural basis of CXCR4 sulfotyrosine recognition by the chemokine SDF-1/CXCL12, *Sci. Signal.* 1 (2008) ra4.
- [71] S.K. Gupta, K. Pillarisetti, Cutting edge: CXCR4-Lo: molecular cloning and functional expression of a novel human CXCR4 splice variant, *J. Immunol.* 163 (1999) 2368–2372.
- [72] Q.Y. Zou, Y.J. Zhao, C. Zhou, A.X. Liu, X.Q. Zhong, Q. Yan, Y. Li, F.X. Yi, I.M. Bird, J. Zheng, G protein alpha subunit 14 mediates fibroblast growth factor 2-induced cellular responses in human endothelial cells, *J. Cell. Physiol.* 234 (2019) 10184–10195.
- [73] T. Cui, F. Leng, Specific recognition of AT-rich DNA sequences by the mammalian high mobility group protein AT-hook 2: a SELEX study, *Biochemistry* 46 (2007) 13059–13066.

- [74] H. Du, J. Zhao, L. Hai, J. Wu, H. Yi, Y. Shi, The roles of vasohibin and its family members: beyond angiogenesis modulators, *Canc. Biol. Ther.* 18 (2017) 827–832.
- [75] G.S. Hossain, J.V. van Thienen, G.H. Werstuck, J. Zhou, S.K. Sood, J.G. Dickhout, A.B. de Koning, D. Tang, D. Wu, E. Falk, R. Poddar, D.W. Jacobsen, K. Zhang, R. J. Kaufman, R.C. Austin, TDAG51 is induced by homocysteine, promotes detachment-mediated programmed cell death, and contributes to the development of atherosclerosis in hyperhomocysteinemia, *J. Biol. Chem.* 278 (2003) 30317–30327.
- [76] M.A. Nagai, Pleckstrin homology-like domain, family A, member 1 (PHLDA1) and cancer, *Biomed Rep* 4 (2016) 275–281.